FCP Report No. 34

# CYCLIC DEFORMATION AND FATIGUE BEHAVIOR OF CARBURIZED STEEL

by

John M. Waraniak
Department of Mechanical and Industrial Engineering

The mechanical behavior of carbon case-hardened components is approached in a systematic manner. Carburized components are viewed as composites of high carbon and low carbon steels. Simulated case and simulated core materials are evaluated separately in homogeneous specimens to determine the independent contributions of each to the overall mechanical behavior. Strain-controlled axial fatigue tests are used to characterize the cyclic deformation and fatigue behavior of case, core and carburized material specimens. The results of these tests are used to correlate the responses of the separate case and core materials to the total mechanical behavior of carburized steel.

A Report of the
FRACTURE CONTROL PROGRAM
College of Engineering, University of Illinois
Urbana, Illinois 61801

May, 1980

# ABSTRACT

The mechanical behavior of carbon case-hardened components is approached in a systematic manner. Carburized components are viewed as composites of high carbon and low carbon steels. Simulated case and simulated core materials are evaluated separately in homogeneous specimens to determine the independent contributions of each to the overall mechanical behavior. Strain-controlled axial fatigue tests are used to characterize the cyclic deformation and fatigue behavior of case, core and carburized material specimens. The results of these tests are used to correlate the responses of the separate case and core materials to the total mechanical behavior of carburized steel.

## ACKNOWLEDGMENT

This investigation was conducted in the Materials Engineering Research Laboratory at the University of Illinois, Urbana-Champaign. The work was supported by the Fracture Control Program, College of Engineering, University of Illinois.

Professor Darrell F. Socie is gratefully acknowledged for many stimulating discussions that have contributed to the author's professional as well as personal development.

Appreciation is due Professor JoDean Morrow for his suggestions, criticism and support, as well as Dr. Gopal Singh, Eaton Corporation, for his interest in, support of the program, and for making available material and specimens.

The author is indebted to Peter Kurath for his many valuable suggestions, comments and assistance throughout the testing program. Special thanks are owed to Mrs. Darlene Mathine for typing the manuscript. Eliot Zaiken and Mark Stanke are also thanked for drafting the figures.

TABLE OF CONTENTS

# LIST OF TABLES

# LIST OF FIGURES

# NOMENCLATURE

| | |
|---|---|
| $\varepsilon$ | True strain |
| $\varepsilon_e$ | Elastic component of strain |
| $\varepsilon_p$ | Plastic component of strain |
| $\varepsilon_f$ | True fracture ductility; true strain at fracture in monotonic tension |
| $\varepsilon_f'$ | Fatigue ductility coefficient; intercept of log $(\Delta\varepsilon_p/2)$ - log $2N_f$ plot at $2N_f = 1$ |
| $\Delta\varepsilon$ | Total strain range |
| $\Delta\varepsilon_e$ | Elastic strain range |
| $\Delta\varepsilon_p$ | Plastic strain range |
| $\sigma$ | True stress |
| $\sigma_a$ | Stress amplitude |
| $\sigma_f$ | True fracture strength; true stress at fracture in monotonic tension |
| $\sigma_f'$ | Fatigue strength coefficient; intercept of log $\sigma_a$ - log $2N_f$ plot at $2N_f = 1$ |
| $\sigma_o$ | Mean stress |
| b | Fatigue strength exponent; slope of log $\sigma_a$ - log $2N_f$ plot |
| c | Fatigue ductility exponent; slope of log $(\Delta\varepsilon_p/2)$ - log $2N_f$ plot |
| E | Modulus of elasticity |
| n | Monotonic strain hardening exponent |
| n' | Cyclic strain hardening exponent |
| $N_f$ | Fatigue life; number of cycles to failure |
| $2N_f$ | Number of reversals to failure |
| $2N_t$ | Transition fatigue life; $2N_f$ when $\Delta\varepsilon_e = \Delta\varepsilon_p$ |
| K | Strength coefficient; true stress to cause a true plastic strain of unity in the relation $\sigma = K(\varepsilon_p)^n$ |
| K' | Cyclic strength coefficient; true stress amplitude to cause a true plastic strain amplitude of unity in the relation $\sigma_a = K'(\Delta\varepsilon_p/2)^{n'}$ |

# I. INTRODUCTION

## A. Background

Carburizing and related thermochemical treatments have become widely accepted as selective surface hardening treatments where atoms are transferred to the surface of the steel at elevated temperatures. Carburizing and selective surface hardening are commonly used to improve the fatigue life and/or wear resistance of steel components. Improvements are related to the increased hardness and strength of the case and to the development of residual compressive stresses in the surface layers after the component has been appropriately quenched and tempered. Mechanical property improvements resulting from selective surface hardening depend complexly upon a variety of metallurgical and mechanical considerations. When surface layers are altered in chemical composition, as in the carburizing process, the transformation kinetics and tempering responses are not the same in the two regions of the resulting composite. Different microstructures result in the case and the core, leading to different responses to deformation.

It has long been appreciated that core toughness is a vital characteristic in the performance of carburized components. In addition, one intuitively senses that a tough, high-hardness case must also contribute substantially to the overall mechanical behavior. The contributions, however, of the individual case and core elements to the total mechanical behavior of the carburized component have been considered in a comprehensive and quantitative manner in relatively few investigations. The mechanical behavior of both the case and the core must be established to identify the separate or independent contributions of each to the overall mechanical behavior.

Although there have been numerous studies directed at evaluating the fatigue resistance of carburized steel and surface-hardened components (1-4)*, there have been relatively few systematic investigations that have led to useful quantitative generalizations. One adopted approach is to view the surface-hardened component as a composite material consisting of a high strength, low ductility case and a lower strength, higher ductility core. This approach has been successfully applied to the analysis of monotonic deformation behavior by Krotine et al (5) and McGuire et al (6), and cyclic deformation behavior by Landgraf and Richman (7,8). The success of this approach in the unrelated monotonic and cyclic deformation investigations indicates that there is considerable merit in this technique. In this investigation Krotine's and Landgraf's work provide a useful starting point for a detailed investigation of the cyclic deformation and fatigue behavior of carburized steel.

As in the previous work, this investigation relies heavily upon separate simulation of case and core materials with homogeneous specimens. Laboratory heats of carburizing grade steels were formulated and remelted to simulate commonly encountered case and core compositions in both Krotine's work and Landgraf's work. This method of material simulation was not used in this investigation. Simulated case material was accomplished by through-carburizing the gage section of specimens and simulated core material was accomplished by pseudo-carburizing specimens. It is important to note that all of the specimens in this investigation were prepared from normalized AISI 8620H steel and that no remelting was employed. Although the high carbon steels in the previous studies simulated metallurgically, the case of carburized components,

*The numbers in parentheses refer to the list of references at the end of the text.

the case material in this investigation was simulated by diffusion of carbon atoms into the steel specimens, just as in the actual carburizing process.

B. Purpose and Scope of Investigation

This investigation is an attempt to approach the surface-hardened component in a systematic manner. Carburized components are regarded as composites of high carbon and low carbon steels. The objective is to study the cyclic deformation and fatigue behavior of carburized steel via separate simulation of case and core compositions and microstructures.

Evaluation of the case and core characteristics may serve to further confirm the usefulness of correlations between responses of the separate case and core materials in predicting the total mechanical behavior of a carburized component. Also, it is hoped that studying the individual mechanical behavior of the case and core material will result in a more precise evaluation of the rheological interactions at the case-core interface.

# II. MECHANICAL BEHAVIOR

## A. Monotonic and Cyclic Deformation Behavior

Metals are metastable under application of cyclic loads. The stress-strain response of metals can be drastically altered due to repeated plastic strain. Depending upon the initial condition of a metal and its test environment, a metal may: (1) cyclically harden, (2) cyclically soften, (3) be cyclically stable, or (4) have mixed behavior (soften or harden, depending on strain range) (9).

Extensive efforts over the past decade have led to major improvements in our ability to characterize the cyclic deformation behavior and fatigue resistance of engineering materials. Central to characterization techniques is a recognition of the importance of the plastic strain component and its role in fatigue damage.

Fatigue damage is caused by cyclic plastic strain and without some plastic strain at localized areas in a structure, failure by fatigue cannot occur (9-12).

Procedures for determining the relevant properties and relations which characterize a material's cyclic behavior are well documented (13,14). Cyclic stress-strain behavior of engineering materials is usually investigated by testing axially loaded, smooth specimens under completely reversed strain cycling. For each cycle in such a test, a stress-strain hysteresis loop, similar to that shown in Fig. 1 is formed. In virtually all engineering metals, hysteresis loops change their proportions as cycling proceeds. If the stress amplitude increases during constant strain-controlled cycling, the metal is said to cyclically harden, whereas the opposite behavior is termed cyclic softening. That is, cyclic hardening means that the resistance

to deformation increases and is evidenced by a decrease in plastic strain with cycles. Cyclic softening is a gradually decreasing resistance to deformation and is reflected as an increase in plastic strain with cycles.

Generally, it can be seen that during cyclic hardening or softening, the cyclically induced changes in stress-strain response occur early in the life, such that the majority of the fatigue life is spent under reasonably stable conditions (15-18). The behavior at half the fatigue life is often taken as representative of the stable behavior. If half-life hysteresis loops from tests at several strain levels are plotted as in Fig. 2, on a single set of axes, the locus of loop tips such as curve OABC, is called the cyclic stress-strain curve (13,19). The cyclic stress-strain curve provides a measure of the steady-state cyclic deformation resistance of a material and it is the cyclic curve that defines the proper stress-strain relation for fatigue analysis.

The cyclic stress-strain curve can be compared directly with the monotonic stress-strain curve to quantitatively assess cyclically induced changes in mechanical behavior. Therefore, the monotonic true stress-strain curve and analysis of tensile data yields useful information such as true fracture strength, ductility and a stress-plastic strain relation of the form:

$$\sigma = K(\varepsilon_p)^n \qquad [1]$$

$\sigma$ = true stress

K = strength coefficient

$\varepsilon_p$ = plastic component of strain

n = monotonic strain hardening exponent

A conventional "engineering" stress-strain curve and a "true" stress-strain curve along with associated properties and parameters, are shown schematically in Fig. 3 (20).

In reference (16), it is shown that the relation between cyclic stress and plastic strain can be described mathematically by a power function similar to that used for the monotonic curve:

$$\sigma_a = K' \left( \frac{\Delta\varepsilon_p}{2} \right)^{n'} \qquad [2]$$

where:

$\sigma_a$ = stable stress amplitude

$K'$ = cyclic strength coefficient

$\Delta\varepsilon_p/2$ = stable plastic strain amplitude

$n'$ = cyclic strain hardening exponent

B. Fatigue Behavior

The culmination of many years of work by cumulative damage fatigue researchers has revealed that the fatigue resistance of metals can be characterized by a strain-life curve. Furthermore, considerable evidence suggests that fatigue failure data is more usefully presented in the form of strain-life curves and strain-based cumulative damage procedures are generally more reliable than the conventional stress-based approaches (9,12,21).

Strain-life curves are usually determined from smooth laboratory specimens that are subjected to constant amplitude, completely reversed strain-controlled cycling. From the resulting hysteresis response as shown in Fig. 1, the relationship between total strain amplitude and reversals to failure can be expressed as the sum of the elastic and plastic components of strain and has the following form:

$$\frac{\Delta\varepsilon}{2} = \frac{\Delta\varepsilon_e}{2} + \frac{\Delta\varepsilon_p}{2} = \frac{\sigma_f'}{E}(2N_f)^b + c_f'(2N_f)^c \qquad [3]$$

where:

$\Delta\varepsilon_e/2$ = elastic strain amplitude

$\Delta\varepsilon_p/2$ = plastic strain amplitude

$\sigma_f'$ = fatigue strength coefficient

$\varepsilon_f'$ = fatigue ductility coefficient

$b$ = fatigue strength exponent

$c$ = fatigue ductility exponent

This relationship is shown schematically in Fig. 4. Several conclusions can be drawn from the total strain-life curve. The relative roles of strength and ductility in resisting fatigue failure at various lives can be gained from knowledge of the transition fatigue life, that is, the life where the total strain amplitude consists of equal plastic and elastic components. At short lives, less than the transition life, lives are governed largely by plastic strain resistance, thus ductility will control performance. At longer lives, greater than the transition life, the elastic strain is more dominant emphasizing the importance of strength. The concept of the transition fatigue life has a great significance in the unified approach to fatigue analysis. That is, the transition fatigue life clearly defines the life region where the plastic strain component dominates, low-cycle fatigue, and the life region where the elastic strain component dominates, high-cycle fatigue. In view of the fact that fatigue damage is caused by cyclic plastic strain, then the only significant difference between various life ranges is the degree of cyclic plasticity. It is generally agreed that a completely elastic analysis of the fatigue behavior of a material is appropriate when considering lives in the range of at least two orders of magnitude beyond the transition fatigue life. Although the high-cycle fatigue behavior of a material may be studied from a completely elastic analysis, it is well to

remember that a portion of the total strain is not elastic whenever a fatigue problem exists.

Strain-controlled axial fatigue testing works best for reasonably ductile, homogeneous, and isotropic materials. Applications of this method of fatigue testing of high hardness steels with controlling internal discontinuities such as nonmetallic inclusions or microcracks may require that one view the steel as a micronotched material (22).

As a result of processing, nonmetallic inclusions are usually the most prevalent microstructural defect present in high-hardness steels; however, in carburized components microcracking may be more important. Considerable evidence suggests that microcracks or microdiscontinuities in an otherwise homogeneous steel matrix, act as stress and strain concentrations and greatly accelerate the crack initiation period in steels (22).

It is not the intent of this investigation to dwell upon the fact that microdiscontinuities in steels of high hardness, such as the simulated case material in this study, are sites of initiation of fatigue cracks and influence the fatigue resistance. Instead, interest is in the mechanical behavior of the case material as an individual element and its contribution to the total mechanical behavior of a carburized component. It is important to acknowledge the fact that microdiscontinuities may be present in the simulated case material of this investigation as well as to appreciate the fact that these microdiscontinuities may also exist in the case material of carburized components.

## C. Structure and Mechanical Behavior

### 1. Microstructure

Despite the many variables (materials, process, etc.) involved in carbon case hardening, all carburized components have in common the fact that

they support a carbon-rich layer at the surface. The goal of the carburizing process is to strengthen the surface of a component with respect to fatigue and wear. In gas carburizing, carbon is taken up by the steel surface in an endothermic atmosphere and then quenched in oil or water. This results in a structure of martensite with varying amounts of retained austenite at the surface and a mixture of martensite with bainite and/or ferrite plus pearlite in the core. Coarseness of the structure is determined by the austenite grain-size prior to quenching (23,24).

Additional microstructural features may also exist along with, or instead of the intended martensite which can significantly influence the mechanical properties of the component. The microstructural features involved are internal oxidation, decarburization, free carbides, retained austenite and microcracks in the martensite (24,25).

Mechanical property improvements that can be developed by carbon case hardening will not be achieved if the surface layers of the carburized component have become internally oxidized or decarburized (24,26,27). Fortunately, internal oxidation and decarburization are restricted to the outer most surface layers; thus, any deleterious effects associated with these surface phenomena can be eliminated by removing the affected layers.

Microcracking, or microscopic cracks across martensitic plates in high carbon steels, has been observed for many years. Microcracking is the result of the impingement of martensite plates during the transformation of austenite. Rauch and Thurtle (28) first identified martensitic microcracks as a possible cause of premature failure in carburized, coarse-grained steels (25). Jena and Heich (29), however, demonstrated that microcracks were also present in fine-grained steels. A systematic investigation by Brobst and Krauss (30) of the relationship between austenitic grain size and microcracking

revealed that microcracking did decrease with decreasing austenitic grain size, but in accord with Jena and Heich, was present to some degree in specimens with grain sizes as fine as ASTM No. 9 (25). The extent to which microcracks might influence the mechanical behavior of carburized steel particularly fatigue crack initiation, is dependent upon surface condition, microcrack size and microcrack distribution. Investigations by Apple and Krauss (25,36) have demonstrated that martensitic microcracks exposed to the surface as a result of polishing laboratory specimens have a significant influence on the fatigue behavior of carburized steel.

Retained austenite is an important metallurgical aspect that must be considered in carburizing steels to higher carbon contents. Although the presence of retained austenite in carburized components has been acknowledged for quite some time, some conflict of opinion regarding its relative importance still exists (25).

When steels are cooled from austenitizing temperatures, austenite becomes unstable and decomposes to some new constituent. The constituent, or transformation product that forms, depends upon the chemical composition of the steel and the cooling rate. When the transformation involves diffusion processes, that is, to form bainite, pearlite or ferrite, the transformation will be complete and no austenite will survive the quench. If the transformation reaction produces martensite, it is possible for some of the austenite to remain in the final microstructure (24).

Investigations by Richman and Landgraf (8) and Krotine et al (5) concluded that the effects of retained austenite are attributable mainly to its mechanical instability. Landgraf found that the important influences of retained austenite for high carbon and case-hardened steels derive from the transformation of austenite during reversed deformation. Landgraf further

concluded that the influence of retained austenite is manifested in cyclic hardening and the development of mean compressive stresses. The cyclic responses originate in the deformation-induced transformation of retained austenite. This induced transformation shear provides a deformation mechanism which is reflected as an increase in ductility and superior fatigue resistance. It is believed that the martensite formed as a result of the deformation-induced transformation of retained austenite is itself more ductile than thermally formed martensite (8).

2. Residual Stresses

It has long been realized that the carburizing process can be accompanied with the development of large residual stresses. The residual stresses can either be detrimental and cause quench cracking, or they can be advantageous and improve the mechanical properties of the carburized steel. Residual stresses arise due to the differences in thermal expansion and contraction of the various phases involved during the carburizing process. Ebert (32) gives an excellent account of the role of residual stresses in the mechanical behavior of carburized steel. Hildenwall and Ericsson (33) have also recently developed computer programs using an incremental step method to compute the residual stress distribution under the surface during and after quenching of a carburized steel.

Assessment of the contribution of the residual stress distribution in carburized steels to the total mechanical behavior is often quite difficult. Despite these difficulties in assessing the quantitative effect of residual stresses on the mechanical behavior of carburized steel, the following observations appear to be demonstrated (32):

(1) The two major principal residual stresses at the surface of the case material in carburized steel are usually

compressive, while the third principal stress which is normal to the surface, is zero at the surface and attains a relatively low tensile value below the surface.

(2) Residual compressive stresses in the surface layers of the case improve the fatigue resistance of carburized steel.

When residual stresses are not appreciably altered during the performance or testing of carburized steel, the residual stresses can be considered equivalent to mean stresses. The following relation proposed by Morrow (34) and verified by Landgraf (35) satisfactorily accounts for the effect of a mean stress on fatigue life:

$$\sigma_a = (\sigma_f' - \sigma_o)(2N_f)^b \qquad [4]$$

It is seen from this relation that a mean stress affects fatigue strength in the same manner as an equivalent change in monotonic fracture strength. The consequences of localizing residual compressive stresses in the surface of carburized components is quite obvious in that a tensile mean stress would reduce the fatigue strength while a compressive mean stress would be beneficial.

# III. EXPERIMENTAL PROGRAM

## A. Material and Specimens

The base material used in this investigation is the case-hardening steel AISI 8620H. Axial specimens were machined from radial sections of forged, normalized gear blanks with a grain size of ASTM No. 9 and prepared according to the dimensions specified in Fig. 5. Specimens were then processed to simulate commonly encountered case and core compositions and microstructures representative of carburized 8620H steel. Material compositions, microstructures, heat treatments and carburizing treatments are given in Table 1.

### 1. Core Material Simulation

Round-uniform-round gage section specimens were processed to simulate the core composition and microstructure commonly encountered in carburized components. Simulation of the core material was accomplished by mock or pseudo-carburizing (36).

Specimens were first copper plated on all surfaces with a copper plate of approximately 0.001 in. thick to prevent carbon from diffusing into the surface. Specimens were then placed in a carburizing oven for eight hours at 1700°F, reheated to 1550°F, quenched in oil and tempered at 300°F for one hour. The copper plate was then electro-chemically stripped from the specimens. Examination of the surface of the stripped specimens revealed no deleterious effects or alterations in surface finish associated with the plating or stripping of the specimens; thus, re-polishing specimens prior to testing was not necessary. Hardness measurements were obtained from Knoop microhardness traverses which were converted to Rockwell C values. Hardness values varied from Rockwell C 45 to 48 and are given in Fig. 6. The microstructure of the

simulated core material was a mixture of martensite and bainite and homogeneous throughout the cross section of the specimen.

2. Case Material Simulation

Round-hourglass gage section specimens were processed to simulate the case composition and microstructure representative of carburized components. Simulation of the case material was accomplished by through-carburizing the gage section of specimens.

Threaded sections of the specimens were copper plated prior to carburizing in order to prevent carburization of these sections. It was desired not to through-carburize the threaded sections of the specimens to prevent embrittlement at the root of the threads and consequent failure in the threads. Specimens were then gas carburized at 1700°F for ten hours in an endothermic atmosphere at a carbon potential of 0.90 to 1.00%. This process was repeated six times for a total of 60 hours. Following the carburization treatment, the specimens were hardened in a neutral salt pot at 1500°F for 15 minutes, then quenched in oil. Specimens were then refrigerated for four hours at -120°F, air-cooled, and tempered at 325°F for two hours. The copper plate was then electrochemically stripped from the threaded sections. To eliminate the effects of surface decarburization and internal oxidation on the test results, a surface layer of 0.0015 in. thick was polished from the surface of the through-carburized specimens. Martensitic microcracks that would have been exposed to the surface of the specimens as a result of polishing were not detected. Microcracks are usually found in microstructures consisting of plate martensite in combination with a substantial amount of retained austenite and relatively large grain size, which is not the condition in this investigation.

Hardness measurements were obtained from Knoop microhardness traverses which were converted to Rockwell C values. Hardness values varied from Rockwell C 58 to 62 and are given in Fig. 6. The microstructure of the simulated case material was martensitic and homogeneous throughout the cross section of the specimen.

Residual stresses and retained austenite content were measured by X-ray diffraction techniques. Volume percent retained austenite in through-carburized specimens was determined by the direct comparison method of Averbach and Cohen using diffracted chromium K-Alpha radiation from the austenite (200), (220) and ferrite (200), (211) planes. The volume percent retained austenite was found to be 3.4 $\pm$ .7%.

Residual stress measurements were made by the two-inclined angle technique employing the diffraction of chromium K-Alpha radiation from the (211) planes of the BCC structure of the 8620H alloy. The residual stress distribution in a through-carburized fatigue specimen prior to final polishing and tempering is shown in Fig. 7. The final polishing and tempering should have effectively minimized the influence of the residual stresses. At high hardnesses and low retained austenite contents which is exactly the condition of the simulated case material in this investigation, a residual stress is equivalent to a mean stress. Therefore, if any residual stresses of significant magnitude remained in the case material specimens after final polishing and tempering, the residual stresses would not change or change only very little due to repeated loading.

In addition to the separate case and core material specimens, a group of round-uniform-round gage section specimens were carburized to a measured case depth of 0.015 in. Specimens were gas carburized at 1650°F in an endothermic atmosphere with a dew point of 25°F for 0.5 hr., cooled

to 1550°F, quenched in oil and tempered at 350°F for 1.0 hr. Threaded sections of these specimens were also copper plated prior to carburizing in order to prevent carburization of these sections. A surface layer of 0.0015 in. was polished from the surface of the specimens and no evidence of microcracking was detected at the surface layers of the specimens. The residual stress distribution in a carburized specimen is shown in Fig. 8.

B. Testing Methods and Approach

Monotonic tension and completely reversed, strain-controlled and load-controlled axial fatigue tests were performed on threaded-end specimens with reduced-diameter, cylindrical and hourglass gage sections. These types and sizes of specimens are typical of those used in strain-controlled, axial low-cycle fatigue testing (37,38). All tests were conducted on a closed-loop servocontrolled hydraulic test system with the capability for accurate measurement, control and recording of loads and strains. Specimen alignment, which is particularly critical for high hardness materials with limited ductility, was accomplished with a liquid-solid, Wood's metal grip similar to that described in reference (37) or ASTM method E606-77T. All tests were performed in laboratory air at room temperature.

The round-hourglass configuration was selected for simulation of the case material in this investigation to circumvent problems associated with the testing of high-hardness steels with limited ductility. It was believed that in processing specimens to high-carbon and low retained austenite contents that the case material would be inherently brittle; thus, monotonic fracture and fatigue failure would occur without any measurable inelastic deformation. A previous investigation by Richman and Landgraf (8) has demonstrated for high-carbon steels designed to simulate the case material

of carburized components that the transition fatigue life of such materials is less than five cycles (ten reversals). This investigation is concerned with life regions ranging from $10^3$ to $10^6$ cycles therefore, a completely elastic analysis of the fatigue behavior of the simulated case material is appropriate. Moreover, assuming that the simulated case material exhibits nearly completely elastic behavior suggests that the fracture mechanism of this material may be controlled by small flaws. Therefore, attempts to monitor crack initiation and early crack growth were also performed. Fatigue crack initiation and early propagation can be monitored on the surface of axially loaded smooth specimens by means of cellulose acetate replicating techniques.

1. Monotonic Deformation Tests

Monotonic tension tests were performed on case material, core material and carburized specimens with reduced-diameter cylindrical gage sections. An axial extensometer was used to monitor and record the monotonic response.

2. Cyclic Deformation Tests

a. Carburized and Core Material

Constant amplitude, completely reversed, strain-controlled axial fatigue tests were performed on carburized and core material specimens with reduced-diameter cylindrical gage sections. An axial extensometer was used to monitor and record the cyclic response. Stress-strain hysteresis loops were recorded at logarithmic intervals during each test to determine the cyclically induced changes in deformation resistance. Fatigue failure was defined as 75% load decay.

Crack initiation and crack growth were monitored on the surface of several specimens by means of cellulose acetate replicas. Replicating tape was softened in acetone and applied to the gage section of the specimen to obtain an impression of the specimen surface. Each crack growth test was interrupted approximately ten times for replicating, and each time it was necessary to take two replicas so as to cover the entire gage section. The procedure employed for obtaining replicas of a specimen in strain control mode is outlined in Appendix A.

b. Case Material

Constant amplitude, completely reversed, load-controlled axial fatigue tests were performed on case material specimens with round-hourglass gage sections. Fatigue failure was defined as complete separation of the specimen into two pieces. Crack initiation and early propagation was monitored on the surface of several specimens by means of cellulose acetate replicas. Each crack growth test was interrupted approximately ten times for replicating, and each time two replicas were taken in order to cover the entire gage section.

# IV. EXPERIMENTAL RESULTS

## A. Monotonic Deformation Behavior

Monotonic tension properties of simulated case, simulated core and carburized material are given in Table 2. Monotonic stress-strain curves for simulated case, core and carburized materials are illustrated in Figs. 9 through 11. True stress-plastic strain curves for simulated core and carburized material are plotted in Figs. 12 and 13. The strength coefficient (K) and strain hardening exponent (n) here calculated by a least-squares curve fit of the data shown in Figs. 12 and 13.

## B. Cyclic Deformation Behavior

Cyclic and fatigue properties of simulated case, simulated core and carburized material are given in Table 3. Cyclic stress-strain curves obtained from companion specimen tests for simulated core and carburized material are shown together with the corresponding monotonic true stress-strain curves in Figs. 10 and 11. The magnitude of cyclic hardening or softening becomes obvious by comparison of the cyclic and monotonic stress-strain curves. Note that the monotonic response of the simulated case material exhibits nearly completely elastic behavior, therefore no measurable plastic strain properties were obtained for this material. Cyclic stress-strain curves for simulated core and carburized materials were obtained by connecting the tips of stable hysteresis loops from several companion specimens tested at different, completely reversed strain levels. Each test was performed at a constant strain amplitude with the loop at approximately half the fatigue life chosen as representative. Figures 14 and 15 contain reproductions of stress-strain hysteresis loops for simulated

core and carburized materials. The cyclic strain hardening exponent (n') and cyclic strength coefficient (K') were calculated by making a least-squares curve fit of the log true stress amplitude versus log true plastic strain amplitude data from companion specimens shown in Figs. 16 and 17. Figure 18 shows a summary plot of monotonic and cyclic stress-strain curves for simulated case, core and carburized materials.

C. Fatigue Behavior

Table 4 summarizes the results of completely reversed load-controlled tests for simulated case material. The results of completely reversed strain-controlled tests for simulated core and carburized materials are given in Tables 5 and 6, respectively. The fatigue strength coefficient ($\sigma_f'$) and fatigue strength exponent (b) were calculated using a least-squares fit to the elastic strain-reversals to failure data assuming that Eq. 3 was valid. The fatigue ductility coefficient ($\varepsilon_f'$) and fatigue ductility exponent (c) were obtained in a similar manner using the plastic strain-reversals to failure data and Eq. 3. Figure 19 shows a logarithmic plot of total strain amplitude versus reversals to failure for the simulated case material. A completely elastic analysis of the fatigue behavior was assumed for the simulated case material, thus the total strain amplitude for this material is assumed to be entirely elastic. Logarithmic plots of elastic, plastic and total strain amplitude versus reversals to failure for simulated core and carburized materials are illustrated in Figs. 20 and 21. The elastic lines for the simulated core and carburized materials show shallower slopes at short lives than at long lives. A single equation relating total strain to life, which adequately fits the fatigue test data for simulated core and carburized materials at all lives, has the following form:

$$\frac{\Delta\varepsilon_t}{2} = \frac{\sigma_f^t}{E}(2N_f)^{b^t} \qquad [5]$$

The values of $(\sigma_f^t)$ and $(b^t)$ are given in Table 3. Figure 22 shows a summary plot of total strain amplitude-reversals to failure data for simulated case, core and carburized materials. Fractographs representative of monotonic tension and fatigue fracture surfaces for simulated case, core and carburized materials are shown in Appendix B.

D. Crack Growth Behavior

Crack growth tests of simulated case material specimens revealed that the majority of life for the case material is spent in fatigue crack initiation. Surface replicas obtained at lives ranging from 80 to 90% of the total fatigue life showed no signs of small cracks. The fact that no surface cracks were observed at these relatively late stages of life suggests that once a fatigue crack has initiated in the case material, rapid unstable crack propagation and final fracture occur rather abruptly or that subsurface crack initiation causes failure. Examination of fracture surfaces of case material specimens showed no signs of subsurface crack initiation.

Crack growth tests of simulated core material specimens indicated that a substantial portion of the total fatigue life of this material is spent in crack initiation. The remaining portion of life is spent in the crack propagation stage consisting of slow stable crack growth followed by rapid unstable crack growth to final fracture. Observations from successive replicas allowed a number of surface cracks to be traced back to lengths of a few thousandths of an inch. Several photographs of replicas showing the progress of fatigue cracks during one simulated core material test are shown

in Appendix A. Crack length-reversals data for this same test are also presented in Appendix A. Quite often more than one crack was observed and final fracture was caused by the joining of these cracks.

Surface replicas obtained from crack growth tests of carburized material specimens showed no signs of surface cracks. As in the crack growth tests of the simulated case material, no small surface cracks were detected in replicas obtained at lives ranging from 80 to 90% of the total fatigue life. Examination of the fracture surfaces of carburized specimens clearly indicated that long-life failure initiated below the surface in carburized specimens. A typical long-life, subsurface failure is shown in the fractograph of a carburized specimen in Appendix B.

No attempts were made to study fatigue crack growth rates. It is important; however, to note that the strain-life behavior of simulated case material is governed by elastic strains and appears to be initiation-dominated at all lives, while the strain-life behavior of simulated core material is governed by elastic strains and appears to be initiation-dominated only at long lives. At short lives, the strain-life behavior of simulated core material is governed largely by plastic strains and appears to be propagation-dominated. In Fig. A-1 it can be seen that at short lives, cracks several thousandths of an inch long were present at less than 50% of the total fatigue life in simulated core material specimens.

# V. ANALYSIS AND DISCUSSION

## A. Stress-Strain Behavior

Stress-strain curves for simulated case, simulated core and carburized material are displayed in Fig. 18. The cyclic curve provides a measure of cyclic deformation resistance, defines the proper stress-strain relation for fatigue analysis, and it is also appropriate for estimating the influence of residual stresses. Cyclically induced changes in stress-strain response generally occur early in life such that the majority of the total fatigue life is spent under stable conditions. Comparison of the cyclic stress-strain curve to the monotonic stress-strain curve for simulated core and carburized materials indicates the magnitude of the cyclically induced changes in these materials. Although the simulated core and carburized material have the same monotonic yield stress, simulated core material experiences cycle-dependent softening under reversed loading which results in a lower cyclic flow curve than that of the carburized material. Carburized material is seen to be cyclically stable. The cyclic behavior observed for simulated core material in this investigation is typical of quenched and lightly tempered steels. That is, nearly stable response or slight softening occurs over the strain-amplitude spectrum, which is consistent with the observations of previous investigations (8,13). Cycle-dependent softening followed by stability are illustrated by the stress-strain hysteresis loops for the simulated core material in Fig. 14.

## B. Cyclic Deformation Behavior

Comparing the stress-strain response of simulated core material shown in Fig. 14 to that of carburized material shown in Fig. 15 reveals an interesting feature. Although the two materials were subjected to the same strain

amplitude, which resulted in nearly identical lives, the cyclic behavior of simulated core material is quite different from that of carburized material. Simulated core material displays typical cycle-dependent softening; however, for carburized material in compression, the tips of successive hysteresis loops are translated upward and parallel to the stress axis, while in tension the tips are relatively stable. The exact reason for the cyclic behavior displayed by the carburized material is not known; however, it appears to be related to the influence of the case region and residual stresses.

Referring to the stress-strain responses displayed in Figs. 14 and 15, it can be seen that the elastic modulus in compression for the simulated core material is nearly identical to the elastic modulus in tension for this material. The elastic modulus in compression, however, is significantly less than the elastic modulus in tension for the carburized material. The apparent higher modulus in tension for carburized material can possibly be explained by residual stress considerations.

On the basis of the residual stress distribution presented in Fig. 8, it can be seen that the major influence of the residual stresses is equivalent to mechanically preloading carburized material specimens. Therefore, when carburized material specimens are subjected to imposed cyclic strains the resultant observed mechanical behavior is the summation of the intrinsic mechanical properties of the material itself and the effects of the residual stresses. When residual stresses are not appreciably altered by subsequent plastic strain, residual stresses are equivalent to mean stresses. Thus it appears the influence of the case region and accompanying compressive residual stresses in this region can possibly account for the apparent higher tension modulus displayed by the carburized material. It is noted for completeness that while the tension modulus is somewhat above the compression

modulus, the net stress-strain response of carburized material to strain cycling is cyclic stability throughout the strain-amplitude spectrum. In terms then of resistance to cyclic loading, the carburized material is more resistant to small strains than the simulated core material.

C. Fatigue Behavior

Axial fatigue results are summarized in the strain-life plot of Fig. 22. Simulated core material is seen to offer superior low-cycle fatigue resistance on the basis of its greater ductility. The stronger simulated case material is superior in the long life regime. Carburized material is seen to have low cycle fatigue resistance intermediate between the simulated case and core material, a common intersection with simulated core material at intermediate lives, and in the long life regime carburized material specimens are more fatigue resistant than either simulated core or case material specimens.

Plotting the strain-life curves for both case and core simulated materials on a common set of axes, as shown in Fig. 22, reveals an interesting feature. Landgraf (7) and Ericsson (23) have both observed that for steels designed to simulate case and core compositions, the strain-life curves of these materials intersected at a life of approximately $2N_f = 10^5$ reversals. This is in agreement with the results of this investigation. Intersection of the life curves for simulated case and core materials accounts for a shift of failure location in carburized components.

In reference (7), Landgraf demonstrated this shift of failure location with carburized axial specimens. At short lives, data points for carburized specimens were intermediate between simulated case and core curves, since in this regime cracks formed in the brittle case region of the carburized specimens early in life and then propagated through the softer core. At the

intersection point, lives for simulated case, simulated core, and carburized materials were nearly identical. In the long life regime, data points for carburized material coincided with the simulated core material curve, which suggested that the core region had become the weaker element. Thus, for carburized material specimens at high strain amplitudes (short lives) cracks start in the case region and surface-initiated failure is expected. At low strain amplitudes (long lives) the case region is more resistant to fatigue. In this regime cracks start in the core region and subsurface-initiated failure is expected.

The cyclic behavior of carburized specimens can be rationalized by viewing carburized specimens as composite materials comprised of two elements: a high strength, low ductility case and a lower strength, higher ductility core (7). Although this is a simplified mechanics view, it is quite reasonable for attempting to analyze and interpret the cyclic behavior observed for carburized material specimens.

It is appreciated that with uniform strain fields, the weakest element of a composite material fails first under reversed loading. If, however, persistent residual stresses can compensate for the differential in resistance to reversed loading, this may not be true. When considering the effect of residual stresses on fatigue, it is important to consider conditions under which residual stresses are cyclically stable (39,40). At short lives, less than the transition fatigue life, residual stresses will relax in the presence of reversed plastic strains. At long lives where behavior is nominally elastic, cyclic stress-relaxation may not appreciably diminish the effects of residual stress. Since the case material is governed largely by elastic strains at all lives, relaxation of residual stresses in the case region of carburized specimens would not occur. The residual stress distribution caused by the

carburizing treatment, as shown in Fig. 8, is compressive near the surface and tensile to some depth below the surface. The effect of compressive residual stresses in the surface layers is to forestall initiation of surface cracks and in the event cracks do form at the surface, they will remain closed unless the externally applied stress can overcome the action of the residual stresses. Elber (41) has shown that a compressive residual stress near the surface caused shallow cracks to grow more slowly than for cases without residual stress. Of course equilibrium conditions require that compressive residual stresses in surface layers must be balanced by tensile stresses elsewhere. Thus a tensile residual stress below the surface caused deeper cracks to grow more rapidly.

D. Low Cycle Fatigue Behavior

It can be seen in Fig. 22 that for shorter lives, $2N_f < 10^3$ reversals, carburized specimens display low cycle fatigue resistance intermediate between simulated case and core materials. It was presumed in the above discussion for carburized material at high strain amplitudes (short lives) that cracks formed in the brittle case region early in life and then propagated through the softer core. Examination of the fracture surfaces of carburized specimens subjected to high strain amplitudes indicated that cracks did indeed start in the case and propagate through the core; however, contrary to the above presumption cracks did not form early in the life. This was confirmed by surface replicas obtained during crack growth tests. Although cracks did initiate at the surface, crack initiation was forestalled for nearly the entire life. The moment a surface crack initiated it was immediately followed by rapid unstable crack propagation to final fracture. It is pertinent to note that at short lives the results of crack

growth tests for simulated core material specimens demonstrated that approximately 50% of the total fatigue life of this material is spent in the crack propagation stage. It appears, however, that the softer core material has no crack arresting effect when unstable fracture occurs in the brittle case region of carburized specimens. This crack growth behavior is consistent with observations reported by Elber (41). That is, when the externally applied stress was sufficient to overcome the action of residual compressive stresses in the case region, the case cracked, forming a deep crack which propagated rapidly through the core. Therefore at short lives the fatigue behavior of carburized specimens would apparently be governed by the intrinsic material properties of the case region and the action of the residual compressive stresses in this region. It should be noted here that residual compressive stresses in the case region would have to be approximately equal to -280 ksi in order to account for the low cycle fatigue behavior observed for carburized specimens in this investigation.

Referring to the residual stress distribution presented in Fig. 8, the average residual stress distribution for both the case and core elements can be estimated. If residual compressive stresses are assumed to be uniformly distributed in the case region, the average residual compressive stress in the case is estimated to be on the order of -30 ksi. Equilibrium conditions would then require the residual tensile stress in the core to be approximately +5 ksi. Assuming a mean stress of -30 ksi and substituting the appropriate simulated case material properties into Eq. 4, it can be shown that the strain-life curve of the simulated case material displayed in Fig. 19 would be shifted upward approximately 10%. Thus, low cycle fatigue behavior observed for carburized specimens in this investigation can in part, be attributed to original residual compressive stresses in the surface layers. It is

important, however, to also consider the effects of retained austenite in surface layers and the rheological interactions between the case and core elements in attempting to rationalize the fatigue behavior of the carburized specimens.

As noted previously, the influence of retained austenite in surface layers of carburized specimens is manifested in cyclic hardening and the development of mean compressive stresses. The transformation of retained austenite to martensite caused by cyclic deformation serves to build a favorable distribution of compressive stresses into the surfaces of carburized specimens (8). Compressive stresses developed as a result of the strain-induced transformation of austenite would then be additive to the original compressive residual stresses in the case; thus, the observed low cycle fatigue behavior for carburized specimens could possibly be explained.

Landgraf and Richman (8) have shown that compressive mean stresses on the order of -30 ksi can be generated by retained austenite transformation; however, as mentioned previously, a mean compressive stress approximately equal to -280 ksi is necessary in order to account for the low cycle fatigue behavior observed for carburized specimens in this investigation.

It is therefore concluded that the original residual compressive stresses and mean compressive stresses generated as a result of retained austenite transformation are not sufficient in magnitude to account for the low cycle fatigue behavior observed for carburized specimens in this investigation. While compressive stresses in surface layers cannot alone account for the low cycle fatigue behavior displayed by carburized specimens, it is believed that rheological interactions between the case and core elements in combination with compressive stresses could possibly explain the observed results.

E. High Cycle Fatigue Behavior

In Fig. 22 it can be seen that for longer lives, $2N_f > 10^4$ reversals, carburized material specimens are more fatigue resistant than either simulated core or case material specimens. The improved resistance to cyclic deformation can possibly be attributed to persistent residual stresses, strain-induced transformation of retained austenite, and rheological interactions between the case and core elements.

Considering the foregoing test results and discussion, it should be noted that for long lives, $2N_f > 10^4$ reversals, subsurface cracks did indeed originate in the core region of carburized specimens. This was confirmed by surface replicas obtained from crack growth tests and the fractographs cited previously. Although long life failures of carburized specimens originated below the surface, in this investigation long life fatigue test data for carburized material do not coincide with long life fatigue data obtained for simulated core material. In the long-life regime, carburized material is more fatigue resistant than either simulated case or core material. It should also be noted here that retained austenite in simulated case material specimens was less than four volume percent, while the volume percent retained austenite in the case region of carburized material specimens was undoubtedly much higher. The effects of retained austenite were presented earlier; however, the major effects of retained austenite in surface layers of carburized specimens appear to be improved fatigue resistance and generation of mean compressive stresses (8).

Since the amount of retained austenite in the core region of carburized specimens is significantly less than that of the case region, any mean compressive stresses generated in the surface layers would have to be balanced by mean tensile stresses in the core (32). Therefore increasing the

compressive stresses in the case region would tend to be detrimental to the core region. While increased tensile stresses in the core region would account for long-life core failures of carburized specimens, the expected decrease in fatigue resistance was not observed. In order to explain the improvement in long-life fatigue resistance observed for carburized specimens in this investigation, it is necessary to consider original residual stresses and stresses generated by retained austenite transformation in combination with rheological interactions between the case and core elements.

In reference (32), Ebert describes a fiber composite simulation model capable of predicting the intensity of the rheological interactions that occur on the axial loading of composites. Although the model was developed to simulate the internal interactions in oriented fiber composite materials, it also duplicates the internal interactions encountered in the axial loading of carburized specimens. Since the case and core have essentially the same elastic constants, they deform as a single unit when a completely elastic strain is applied to a carburized specimen loaded in simple uniaxial tension. Furthermore, since the case and core deform as a single integral unit, the only stresses generated are those in the axial direction, which are uniformly distributed. If, however, the applied strain is not completely elastic and is sufficient to cause plastic flow in the softer core while the hard case is still behaving elastically, the core would contract diametrally more than the case because the Poisson ratio of the core exceeds that of its elastic value. As a result, transverse stresses are generated in the radial and circumferential directions. The transverse stresses generated in the circumferential direction are compressive near the surface and tensile in the core, therefore they resemble the original residual stresses encountered in carburized specimens. Specifically, loading a carburized specimen in tension

can, if the load is high enough, cause the core to flow plastically at stresses where the case is behaving elastically. Because of the difference in Poisson's ratio for elastic (about 0.3) and plastic flow (0.5), the case and core have different contracting tendencies which result in the development of transverse stresses. The transverse stresses tend to restrict the flow of the softer core thereby producing a multiaxial stress state which raises the over-all flow stress of the carburized specimen. Thus, multiaxial stresses developed at the case-core interface would enhance the long-life fatigue resistance of carburized specimens. It should be noted here that the multiaxial stress state developed at the case-core interface would also act as an embrittling agent thus, a tough core is essential, since at the interface the reaction of the core material dominates that of the case which has a beneficial compressive stress.

# VI. CONCLUSIONS

1. Carburized axial specimens can be viewed as composites when subjected to uniaxial tension and compression. This simplified mechanics view has considerable merit in assessing how the cyclic responses of surface layers in carburized specimens contribute to the overall fatigue behavior.

2. Contributions of the individual case and core elements to the total cyclic behavior of carburized specimens cannot alone account for the synergistic increase in resistance to cyclic deformation.

3. The results of this investigation tend to support the usefulness of correlations between the responses of the separate case and core materials and the behavior of carburized specimens. While contributions of the individual case and core elements are necessary to quantitatively assess the fatigue behavior of carburized specimens, they are not sufficient. Multiaxial stresses developed at the case-core interface, residual stresses caused by the carburizing process, and mean stresses generated by the deformation-induced transformation of retained austenite must be considered in combination with the separate responses of case and core materials in attempting to rationalize the total cyclic behavior of carburized specimens.

4. Original residual stresses and mean stresses generated by retained austenite transformation did not explain the fatigue behavior observed for carburized specimens in this investigation; however, they may contribute significantly to the multiaxial stress state developed at the case-core interface.

# REFERENCES


1. Bidwell, J. B. et al, "Fatigue Durability of Carburized Steel," American Society for Testing Materials, Cleveland, Ohio, 1957.

2. Love, R. J., Proceedings, Symposium on Properties of Metallic Surfaces, Institute of Metals, 1953, p. 161.

3. Roberts, J. G. and Mattson, R. L., "Fatigue Durability of Carburized Steel," American Society for Metals, 1957, p. 68.

4. De Paul, R. A., "Metals Engineering Quarterly," Vol. 10, 1970, p. 25.

5. Krotine, F. T., McGuire, M. F., Ebert, L. J. and Troiano, A. R., "Transactions," American Society for Metals, Vol. 62, 1969, p. 829.

6. McGuire, M. F., Troiano, A. R. and Ebert, L. J., "Transactions," Series D, American Society of Mechanical Engineers, Vol. 93, 1971, p. 699.

7. Landgraf, R. W. and Richman, R. H., "Fatigue Behavior of Carburized Steel," Fatigue of Composite Materials, ASTM STP 569, American Society for Testing Materials, 1975, pp. 130-144.

8. Richman, R. H. and Landgraf, R. W., "Some Effects of Retained Austenite on the Fatigue Resistance of Carburized Steel," Metallurgical Transactions A, Vol. 6A, No. 5, 1975, pp. 955-964.

9. Socie, D. F., Mitchell, M. R. and Caulfield, E. M., "Fundamentals of Modern Fatigue Analysis," Fracture Control Program Report No. 26, University of Illinois, College of Engineering, Urbana, Illinois, April, 1977.

10. Sandor, B. I., "Fundamentals of Cyclic Stress and Strain," University of Wisconsin Press, Madison, Wisconsin, 1972.

11. ASTM STP 519, "Cyclic Stress-Strain Behavior-Analysis, Experimentation and Failure Prediction," edited by L. F. Coffin and E. Krempl, American Society for Testing and Materials, Philadelphia, Pennsylvania, 1973.

12. Landgraf, R. W. and Wetzel, R. M., "Cyclic Deformation and Fatigue Damage," Proceedings, International Conference on Mechanical Behavior of Materials, Vol. II, Kyoto, Japan, 1972.

13. Landgraf, R. W., Morrow, JoDean and Endo, T., "Determination of the Cyclic Stress-Strain Curve," Journal of Materials, Vol. 4, 1969, p. 176.

14. Manual on Low Cycle Fatigue Testing, ASTM STP 465, American Society for Testing Materials, 1969.

15. Smith, R. W., Hirschberg, M. H. and Manson, S. S., "Fatigue Behavior of Materials under Strain Cycling in Low and Intermediate Life Range," NASA TN D-1574, National Aeronautics and Space Administration, Washington, D. C., April, 1963.

16. Morrow, J., "Cyclic Plastic Strain Energy and Fatigue of Metals," Internal Friction, Damping and Cyclic Plasticity, STP 378, American Society for Testing and Materials, 1965, pp. 45-87.

17. Landgraf, R. W., "Cyclic Deformation and Fracture of Hardened Steels," International Conference on Mechanical Behavior of Materials," Kyoto, Japan, 1972.

18. Landgraf, R. W., "The Resistance of Metals to Cyclic Deformation," Achievement of High Fatigue Resistance in Metals and Alloys, STP 467, American Society for Testing and Materials, 1970, pp. 3-36.

19. Dowling, N. E., "Stress-Strain Analysis of Cyclic Plastic Bending and Torsion," Journal of Engineering Materials and Technology, Vol. 100, April, 1978, pp. 157-163.

20. Raske, D. T. and Morrow, JoDean, "Mechanics of Materials in Low Cycle Fatigue Testing," Manual on Low Cycle Fatigue Testing, ASTM STP 465, American Society for Testing and Materials, 1969, pp. 1-25.

21. Dowling, N. E., "Fatigue Failure Predictions for Complicated Stress-Strain Histories," Journal of Materials, Vol. 7, 1971, p. 71.

22. Mitchell, M. R., "A Unified Predictive Technique for the Fatigue Resistance of Cast Ferrous-Based Metals and High Hardness Wrought Steels," Fracture Control Program Report No. 23, University of Illinois, College of Engineering, Urbana, Illinois, September, 1976.

23. Ericsson, Torsten, "New Developments in Thermochemical Heat Treatments of Steel," Department of Mechanical Engineering, Linköping University, Särtryck ur, "Nya material for avancerad teknik," Jubileums symposium vid Kth, Stockholm, June 7-8, 1977.

24. Parrish, G., "The Influence of Microstructure on the Properties of Case-Carburized Components"
Heat Treatment of Metals, 3 (1976):1, 6-11
" " " " , 3 (1976):2, 49-53
" " " " , 3 (1976):3, 73-78
" " " " , 3 (1976):4, 101-109
" " " " , 4 (1977):1, 17-27

25. Krauss, G., "The Microstructure and Fracture of a Carburized Steel," Met. Trans. A., Vol. 9A, No. 11, 1978, p. 1527.

26. Magnusson, L., "Fatigue of Case-Hardened Steel," Proceedings, Fatigue-Fundamental and Applied Aspects, Saabgarden, Rimforsa, Sweden, August, 1977.

27. Magnusson, L., Utmattning av ythärdat material, Lith-IKP-R-80, University of Linköping, 1976.

28. Rauch, A. H. and Thurtle, W. R., Metal Progress, Vol. 69, 1956, p. 73.

29. Jena, L. and Heich, P., "Microcracks in Carburized and Hardened Steel," Met. Trans., Vol. 3, February, 1972, p. 588.

30. Brobst, R. P. and Krauss, G., Met. Trans., Vol. 5, 1974, p. 457.

31. Apple, C. A. and Krauss, G., "Microcracking and Fatigue in a Carburized Steel," Met. Trans., Vol. 4, May, 1973, p. 1195.

32. Ebert, L. J., "The Role of Residual Stresses in the Mechanical Performance of Case Carburized Steels," Met. Trans., Vol. 9A, November, 1978, p. 1537-1551.

33. Hildenwall, B. and Ericsson, T., "Prediction of Residual Stresses in Case-Hardening Steels," Hardenability Concepts with Applications to Steel, Proceedings of a Symposium held at the Sheraton-Chicago Hotel, October 24-26, 1977.

34. Morrow, JoDean, "Fatigue Properties of Metals," unpublished draft submitted to the Fatigue Design Committee of SAE ISTC Division 4, April, 1964.

35. Landgraf, R. W., "Effect of Mean Stress on the Fatigue Behavior of a Hard Steel," Master's Thesis, Department of Theoretical and Applied Mechanics, University of Illinois, 1966.

36. Carburizing and Carbonitriding, ASM Committee on Gas Carburizing, Metals Park, Ohio, ASM, 1977.

37. Feltner, C. E. and Mitchell, M. R., "Basic Research on the Cyclic Deformation and Fracture Behavior of Materials," Manual on Low Cycle Fatigue Testing, STP 465, American Society for Testing Materials, 1969, pp. 27-66.

38. ASTM Recommended Practice for Constant-Amplitude Low-Cycle Fatigue Testing (E606-77T).

39. Morrow, J., Ross, A. S. and Sinclair, G. M., "Relaxation of Residual Stresses Due to Fatigue Loading," SAE Trans., Vol. 68, 1960.

40. Landgraf, R. W. and Francis, R. C., "Material and Processing Effects on Fatigue Performance of Leaf Springs," SAE Technical Paper Series, 1979.

41. Elber, W., "Effects of Shot-Peening Residual Stresses on the Fracture and Crack-Growth Properties of D6AC Steel," ASTM STP 559, 1974.

TABLE 1

MATERIAL COMPOSITIONS AND PROCESSING

| Material | C | S | P | Mn | Si | Cr | Ni | Mo |
|---|---|---|---|---|---|---|---|---|
| Base | 0.22 | 0.029 | 0.005 | 0.83 | 0.24 | 0.50 | 0.41 | 0.15 |
| Core | 0.22 | 0.027 | 0.024 | 0.81 | 0.15 | 0.56 | 0.43 | 0.15 |
| Case | 0.72 | 0.029 | 0.016 | 0.78 | 0.17 | 0.64 | 0.49 | 0.17 |

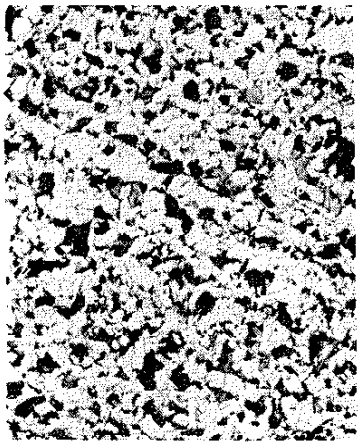

Base Material
HRB 82
100X

Simulated Core Material
HRC 47
500X

Simulated Case Material
HRC 61
500X

Processing

Core: Pseudo-carburized at 1700°F, reheated to 1550°F, quenched in oil, and tempered at 300°F for one hour.

Case: Carburized at 1700°F in an endothermic atmosphere for ten hours, carbon potential of .90 to 1.00%, process repeated six times. Hardened in a neutral salt pot at 1500°F for 15 minutes, quenched in oil, refrigerated for four hours at -120°F, air cooled, and tempered at 325°F for two hours.

Carburized: Carburized at 1650°F in an endothermic atmosphere with a dew point of 25°F for 0.5 hours, coded to 1550°F, quenched in oil and tempered at 350°F for one hour.

TABLE 2

MECHANICAL PROPERTIES OF SIMULATED CASE, SIMULATED CORE, AND CARBURIZED MATERIALS

| MATERIAL | CASE | CORE | CARBURIZED |
|---|---|---|---|
| Modulus of Elasticity, E, x $10^5$ MPa (x $10^3$ ksi) | 1.93 (28.0) | 1.98 (28.8) | 1.95 (28.3) |
| 0.2% Offset Yield Strength, MPa (ksi) | NA* | 1200 (174) | 1200 (174) |
| Ultimate Tensile Strength, Su, MPa (ksi) | 1600 (232) | 1510 (219) | 1586 (230) |
| Percent Reduction in Area, %RA | NIL | 42.2 | 2.6 |
| True Fracture Strength, $\sigma_f$, MPa (ksi) | 1600 (232) | 2034 (295) | 1669 (242) |
| True Fracture Ductility, $\varepsilon_f$ | 0.0085 | 0.549 | 0.026 |
| Strain Hardening Exponent, n | NIL | 0.094 | 0.129 |
| Strength Coefficient, K, MPa (ksi) | NA | 2151 (312) | 2668 (387) |

*Not applicable

TABLE 3

CYCLIC AND FATIGUE PROPERTIES OF SIMULATED CASE, SIMULATED CORE AND CARBURIZED MATERIALS

| MATERIAL | CASE | CORE | CARBURIZED |
|---|---|---|---|
| Cyclic Yield Strength, 0.2% Offset, MPa (ksi) | NA* | 1082 (157) | 1213 (176) |
| Cyclic Strain Hardening Exponent, $n'$ | NIL | 0.116 | 0.139 |
| Cyclic Strength Coefficient, $K'$, MPa (ksi) | NA | 2220 (322) | 2875 (417) |
| Fatigue Strength Coefficient, $\sigma_f'$, MPa (ksi) | 1931 (280) | 2510 (364) | 2344 (340) |
| Fatigue Ductility Coefficient, $\varepsilon_f'$ | NIL | 0.053 | 0.027 |
| Fatigue Strength Exponent, b | -0.109 | -0.116 | -0.097 |
| Fatigue Ductility Exponent, c | NA | -0.444 | -0.398 |
| Transition Fatigue Life, $2N_t$, Reversals | NA | 79 | 15 |
| Fatigue Strength Coefficient** $\sigma_f^t$ MPa (ksi) | NA | 7943 (1152) | 4488 (651) |
| Fatigue Strength Exponent*** $b^t$ | NA | -0.224 | -0.152 |

*Not applicable

**Fatigue strength coefficient relating total strain to life

***Fatigue strength exponent relating total strain to life

TABLE 4

STRAIN-LIFE DATA FOR COMPLETELY REVERSED LOAD CONTROLLED TESTS
SIMULATED CASE MATERIAL

| SPECIMEN NO. | TOTAL LOAD AMPLITUDE $\Delta P/2$ KN (LBS) | TOTAL STRESS AMPLITUDE $\Delta\sigma/2$ MPa (KSI) | TOTAL STRAIN AMPLITUDE $\Delta\varepsilon/2$ | REVERSALS TO FAILURE $2N_f$ |
|---|---|---|---|---|
| D79-15 | 23.7 (5330) | 1158 (168) | 6.00 E-3 | 8.20 E+1 |
| D79-05 | 19.6 (4400) | 965 (140) | 5.00 E-3 | 8.76 E+2 |
| D79-12 | 19.6 (4400) | 965 (140) | 5.00 E-3 | 1.22 E+3* |
| D79-20 | 19.6 (4400) | 965 (140) | 5.00 E-3 | 3.01 E+3* |
| D79-06 | 17.7 (3990) | 870 (126) | 4.50 E-3 | 4.97 E+3 |
| D79-16 | 15.7 (3530) | 772 (112) | 4.00 E-3 | 6.59 E+3* |
| D79-17 | 15.7 (3530) | 772 (112) | 4.00 E-3 | 6.61 E+3 |
| D79-08 | 15.7 (3530) | 772 (112) | 4.00 E-3 | 1.11 E+4 |
| D79-07 | 13.8 (3100) | 676 (98) | 3.50 E-3 | 1.46 E+4 |
| D79-18 | 11.8 (2650) | 579 (84) | 3.00 E-3 | 1.97 E+4 |
| D79-19 | 11.8 (2650) | 579 (84) | 3.00 E-3 | 3.22 E+4 |
| D79-13 | 11.8 (2650) | 579 (84) | 3.00 E-3 | 3.46 E+4 |
| D79-04 | 9.8 (2200) | 483 (70) | 2.50 E-3 | 7.33 E+4 |
| D79-09 | 9.8 (2200) | 483 (70) | 2.50 E-3 | 1.31 E+5 |
| D79-22 | 9.8 (2200) | 483 (70) | 2.50 E-3 | 2.00 E+6† |
| D79-21 | 7.9 (1770) | 386 (56) | 2.00 E-3 | 2.00 E+6† |

*Crack growth test

†Did not fail

TABLE 5

STRAIN-LIFE DATA FOR COMPLETELY REVERSED STRAIN CONTROLLED TESTS
SIMULATED CORE MATERIAL

| SPECIMEN NO. | TOTAL STRAIN AMPLITUDE $\Delta\varepsilon/2$ | TOTAL STRESS AMPLITUDE $\sigma_a$ MPa (KSI) | PLASTIC STRAIN $\Delta\varepsilon_p/2$ | ELASTIC STRAIN $\Delta\varepsilon_e/2$ | REVERSALS TO FAILURE $2N_f$ |
|---|---|---|---|---|---|
| D79-46 | 1.01 E-2 | 1193 (173) | 4.17 E-3 | 5.93 E-3 | 2.28 E+2 |
| D79-33 | 1.01 E-2 | 1172 (170) | 4.04 E-3 | 6.06 E-3 | 4.88 E+2 |
| D79-31 | 7.02 E-3 | 1041 (151) | 1.78 E-3 | 5.24 E-3 | 1.94 E+3* |
| D79-45 | 7.07 E-3 | 1055 (153) | 1.47 E-3 | 5.60 E-3 | 1.98 E+3 |
| D79-39 | 7.07 E-3 | 1034 (150) | 1.58 E-3 | 5.49 E-3 | 3.16 E+3 |
| D79-27 | 5.05 E-3 | 910 (132) | 5.00 E-4 | 4.55 E-3 | 9.18 E+3 |
| D79-34 | 5.08 E-3 | 917 (133) | 4.50 E-4 | 4.63 E-3 | 9.60 E+3* |
| D79-42 | 5.05 E-3 | 917 (133) | 4.30 E-4 | 4.62 E-3 | 1.19 E+4 |
| D79-36 | 4.04 E-3 | 793 (115) | 5.00 E-5 | 3.99 E-3 | 1.96 E+4* |
| D79-29 | 4.05 E-3 | 779 (113) | 1.00 E-4 | 3.95 E-3 | 2.10 E+4 |
| D79-30 | 4.05 E-3 | 800 (116) | 7.00 E-5 | 3.98 E-3 | 2.60 E+4 |
| D79-40 | 3.03 E-3 | 607 (88) | NIL | 3.03 E-3 | 1.14 E+5 |
| D79-38 | 3.03 E-3 | 593 (86) | NIL | 3.03 E-3 | 1.50 E+5 |
| D79-28 | 2.02 E-3 | 407 (59) | NIL | 2.02 E-3 | 3.31 E+5 |
| D79-47 | 2.03 E-3 | 407 (59) | NIL | 2.03 E-3 | 9.30 E+5 |

*Crack growth test

TABLE 6

STRAIN-LIFE DATA FOR COMPLETELY REVERSED STRAIN CONTROLLED TESTS
CARBURIZED MATERIAL

| SPECIMEN NO. | TOTAL STRAIN AMPLITUDE $\Delta\varepsilon/2$ | TOTAL STRESS AMPLITUDE $\sigma_a$ MPa (KSI) | PLASTIC STRAIN $\Delta\varepsilon_p/2$ | ELASTIC STRAIN $\Delta\varepsilon_e/2$ | REVERSALS TO FAILURE $2N_f$ |
|---|---|---|---|---|---|
| D79-50 | 1.01 E-2 | 1338 (194) | 3.23 E-3 | 6.87 E-3 | 2.02 E+2* |
| D79-67 | 7.07 E-3 | 1103 (160) | 1.25 E-3 | 5.82 E-3 | 1.80 E+3 |
| D79-68 | 7.07 E-3 | 1103 (160) | 1.30 E-3 | 5.77 E-3 | 2.33 E+3 |
| D79-54 | 7.08 E-3 | 1138 (165) | 1.25 E-3 | 5.83 E-3 | 3.40 E+3* |
| D79-69 | 5.04 E-3 | 903 (131) | 3.10 E-4 | 4.73 E-3 | 1.32 E+4 |
| D79-70 | 5.05 E-3 | 924 (134) | 2.70 E-4 | 4.78 E-3 | 2.07 E+4 |
| D79-56 | 5.06 E-3 | 945 (137) | 2.20 E-4 | 4.84 E-3 | 2.32 E+4* |
| D79-65 | 4.03 E-3 | 772 (112) | 4.00 E-5 | 3.99 E-3 | 9.63 E+4 |
| D79-58 | 4.04 E-3 | 772 (112) | 1.00 E-5 | 4.03 E-3 | 1.23 E+5* |
| D79-61 | 4.04 E-3 | 786 (114) | 3.00 E-5 | 4.01 E-3 | 1.40 E+5 |
| D79-57 | 3.02 E-3 | 593 (86) | NIL | 3.02 E-3 | 2.50 E+5$^{\nabla\dagger}$ |
| D79-55 | 3.04 E-3 | 614 (89) | NIL | 3.04 E-3 | 4.10 E+5$^{\dagger}$ |
| D79-59 | 3.04 E-3 | 641 (93) | NIL | 3.04 E-3 | 8.57 E+5$^{\dagger}$ |

*Crack growth test

$^{\nabla}$Refrigerated in liquid nitrogen

$^{\dagger}$Failed in the threads

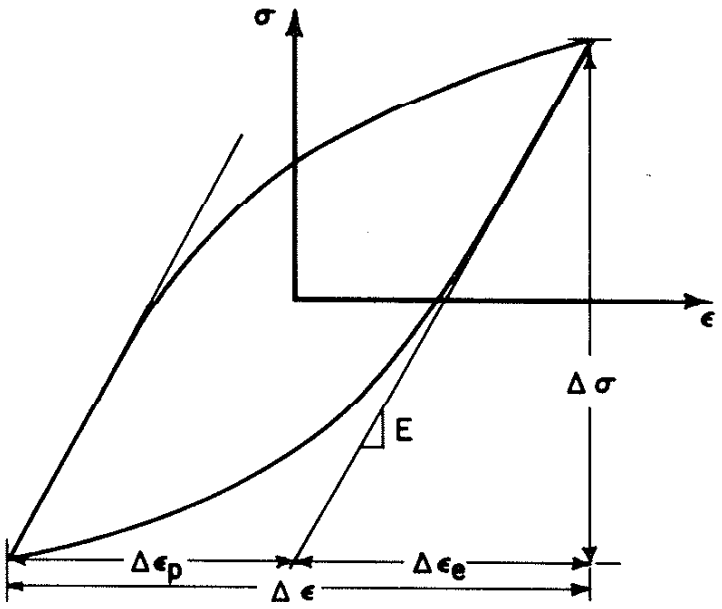


FIG. 1 STRESS-STRAIN HYSTERESIS LOOP AND CHARACTERIZING PARAMETERS

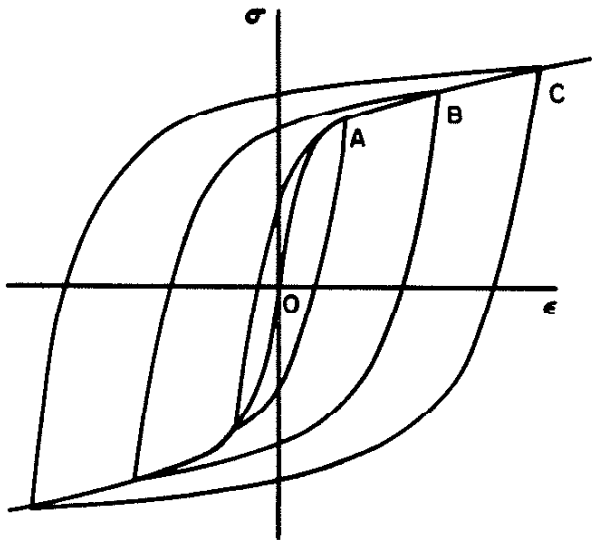


FIG. 2 CYCLIC STRESS-STRAIN CURVE DRAWN THROUGH STABLE LOOP TIPS

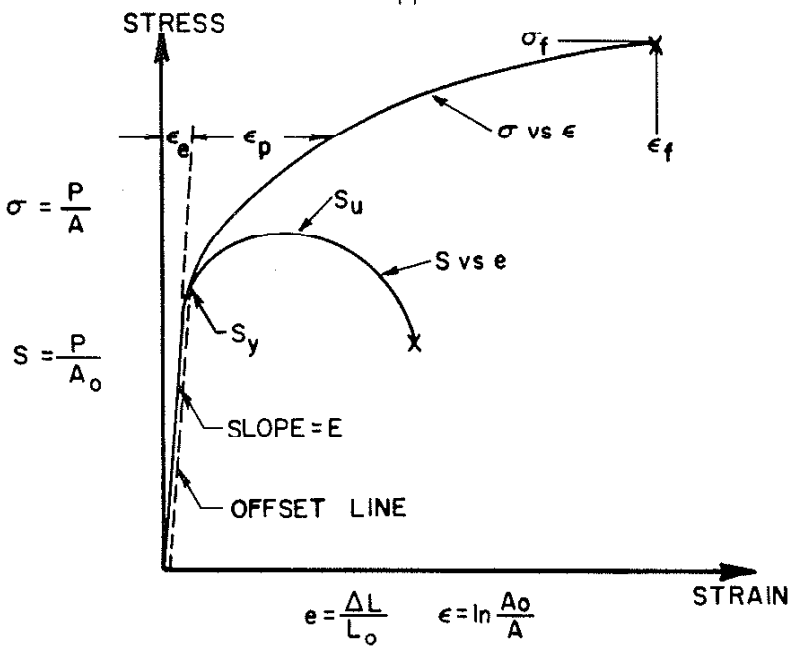


FIG. 3 ENGINEERING AND TRUE STRESS-STRAIN CURVES WITH CHARACTERIZING PARAMETERS

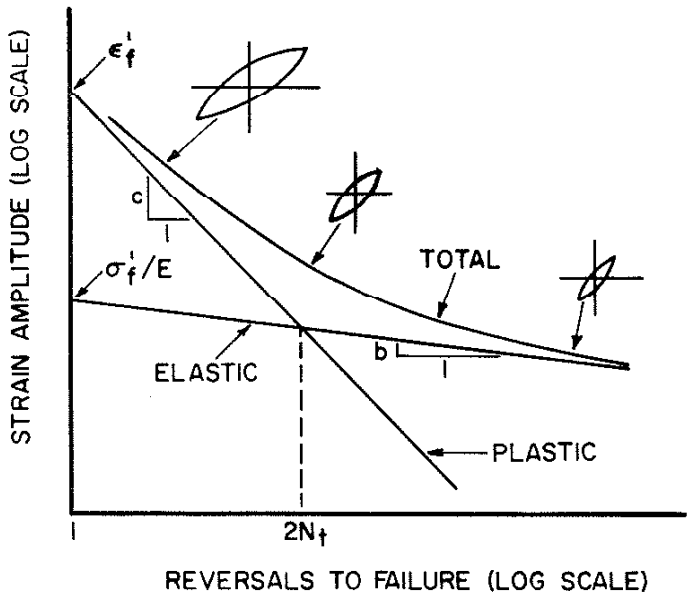


FIG. 4 SCHEMATIC REPRESENTATION OF STRAIN AMPLITUDE-FATIGUE LIFE RELATION

1)

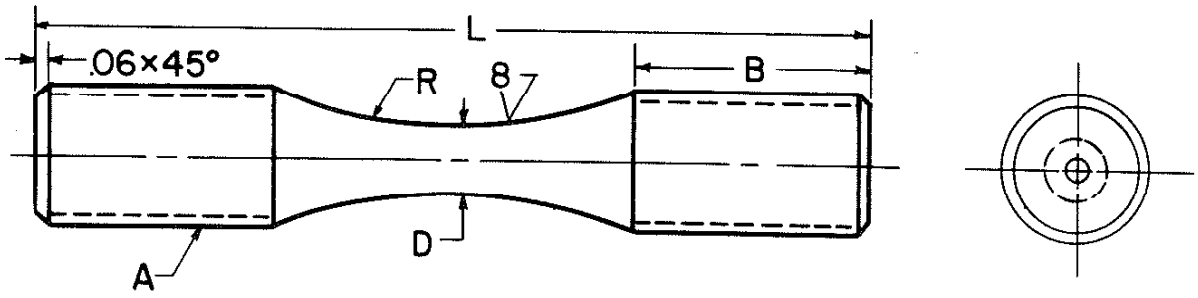


2)

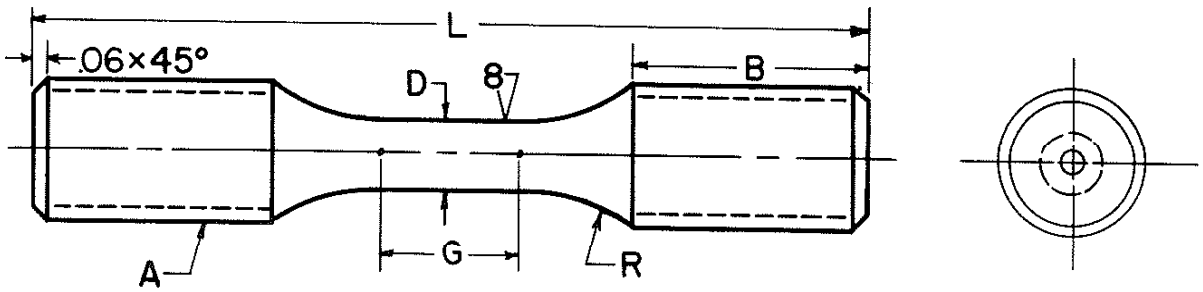


| DIMENSIONS (INCHES) | | | | | | |
|---|---|---|---|---|---|---|
| SPECIMEN NO. | A | B | D | G | L | R |
| SPECIMEN 1 | 7/16-20 UNF | 0.600 | 0.200 | —— | 2.60 | 1.60 |
| SPECIMEN 2 | 7/16-20 UNF | 0.500 | 0.200 | 0.500 | 2.60 | 1.20 |
| | —— | REF | ±.001 | ±.005 | MIN | ±.01 |

NOTES:

1) BLEND RADIUS R NOT TO UNDERCUT DIMENSION D.
2) DIMENSION D CONCENTRIC TO THREAD WITHIN 0.002.
3) DIMENSIONS G & R TO BE CENTRAL TO L WITHIN 0.05.
4) SPECIMEN TEMPERATURE NOT TO EXCEED 212°F DURING MACHINING.

FIG. 5 LABORATORY TEST SPECIMENS

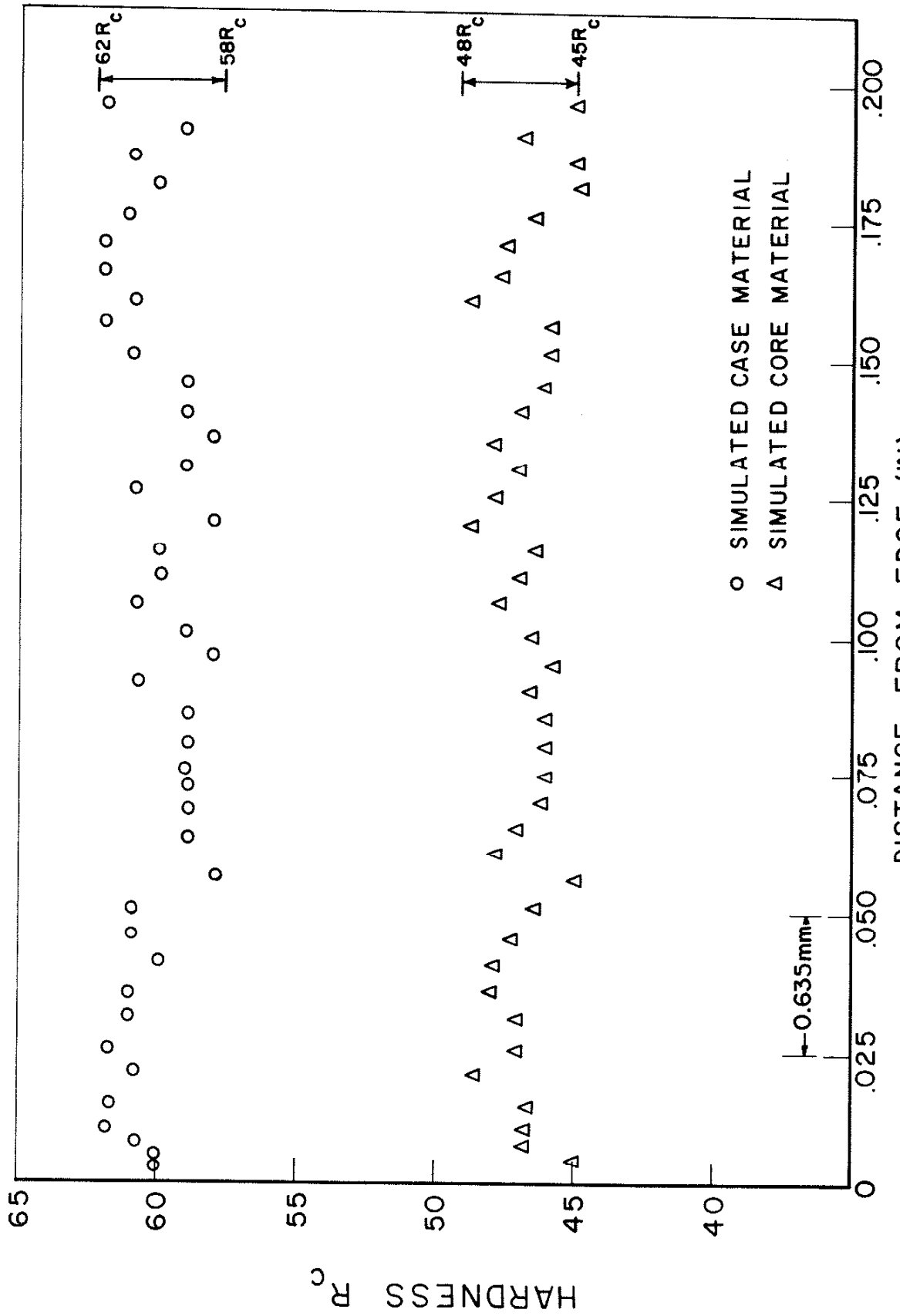


FIG. 6 CROSS-SECTION HARDNESS TRAVERSES

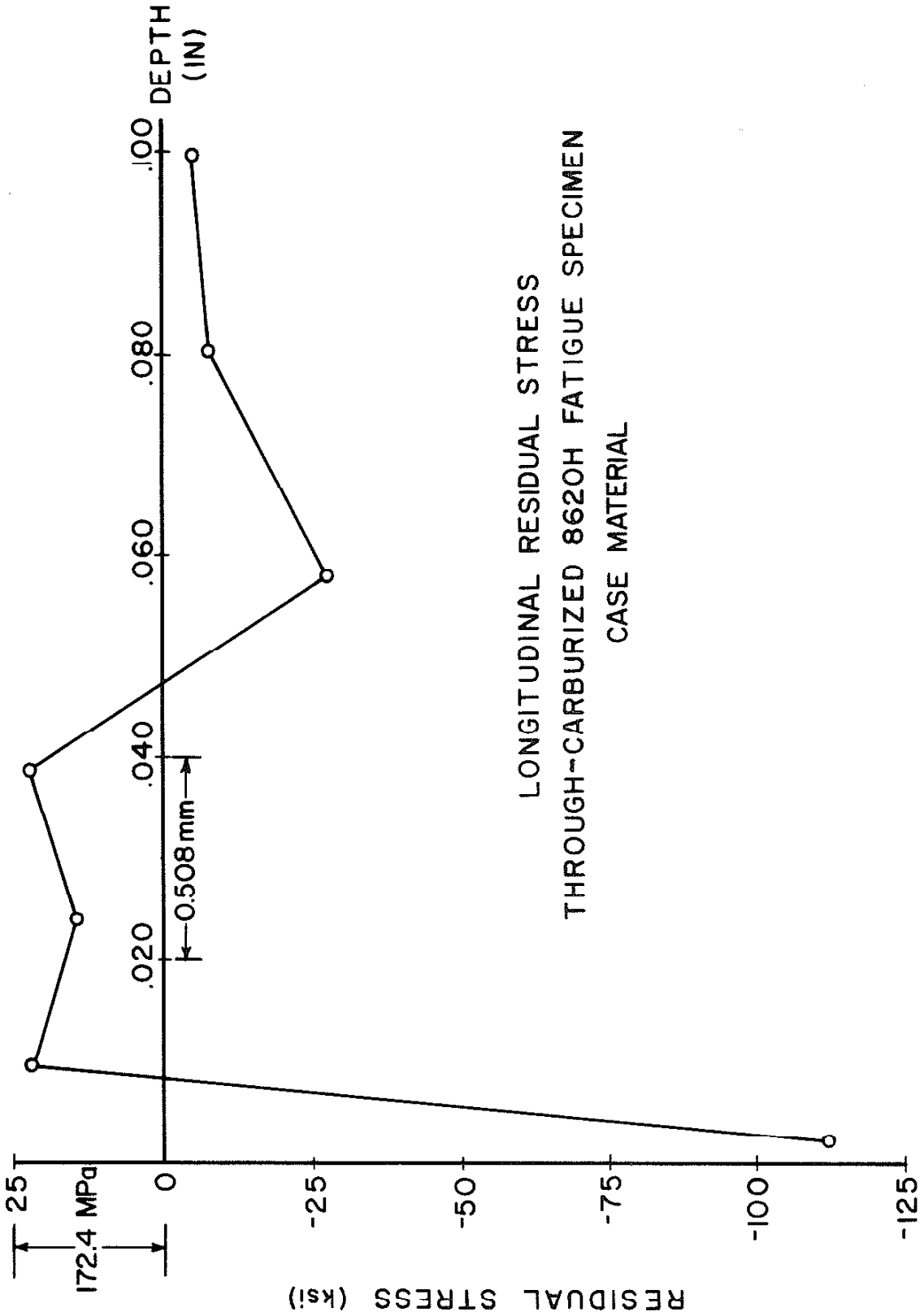


FIG. 7 X-RAY DIFFRACTION RESIDUAL STRESS ANALYSIS-SIMULATED CASE MATERIAL

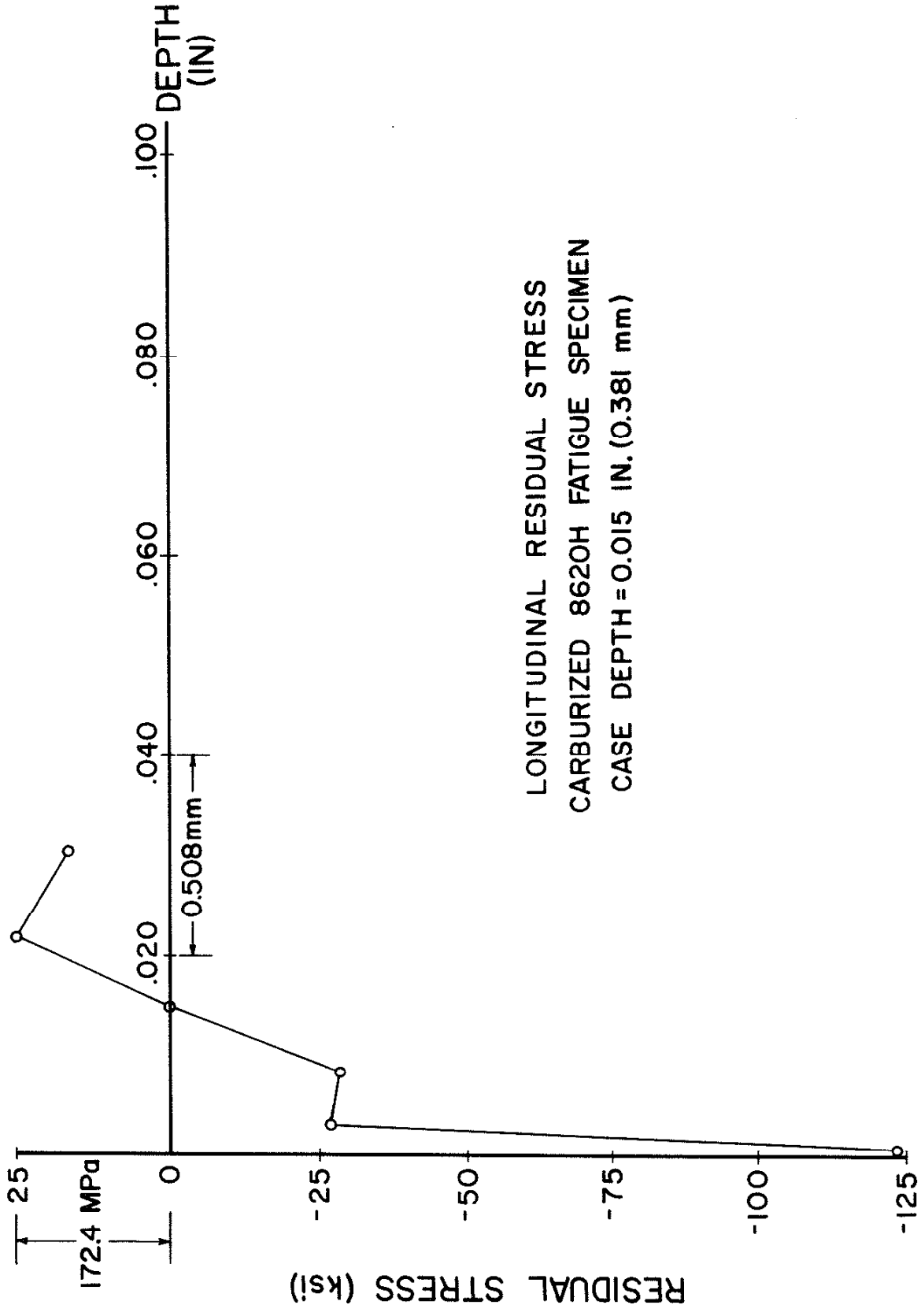


FIG. 8 X-RAY DIFFRACTION RESIDUAL STRESS ANALYSIS-CARBURIZED MATERIAL

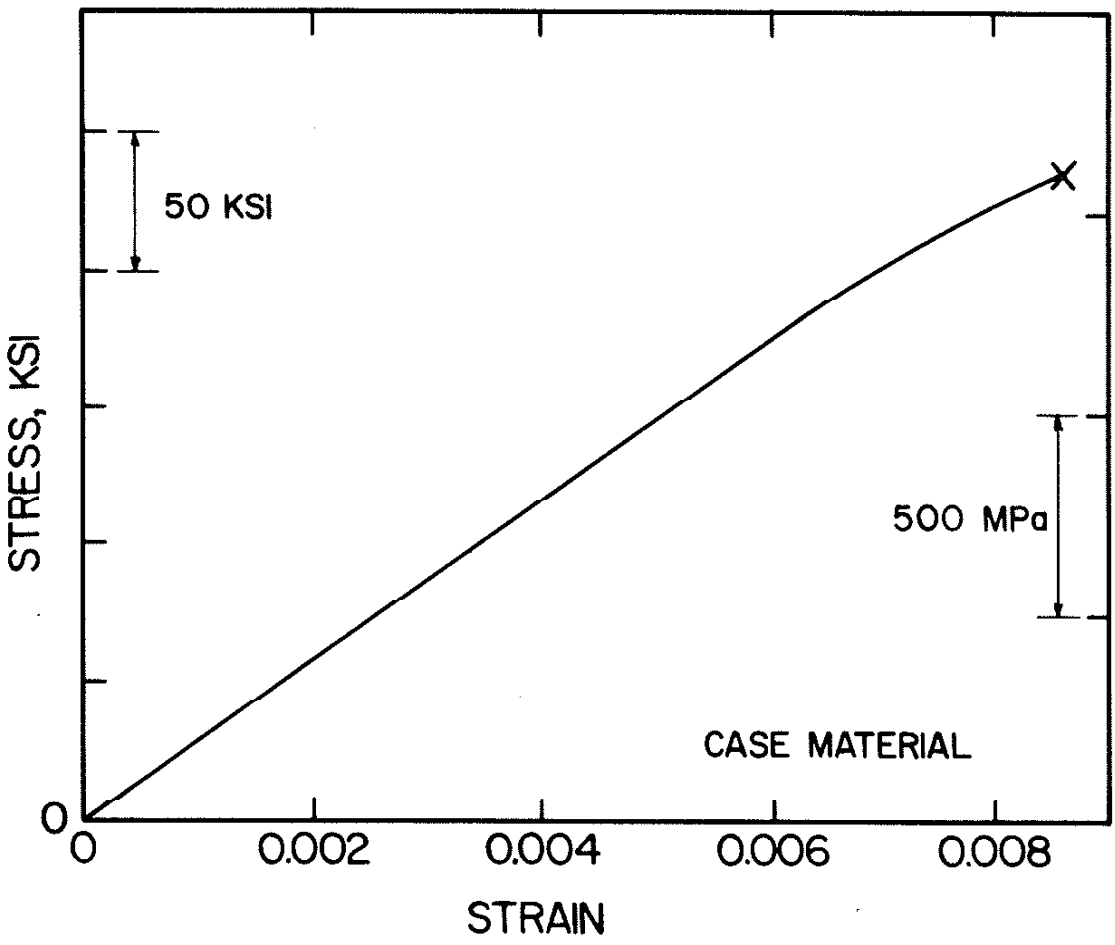


FIG. 9 MONOTONIC STRESS-STRAIN CURVE FOR SIMULATED CASE MATERIAL

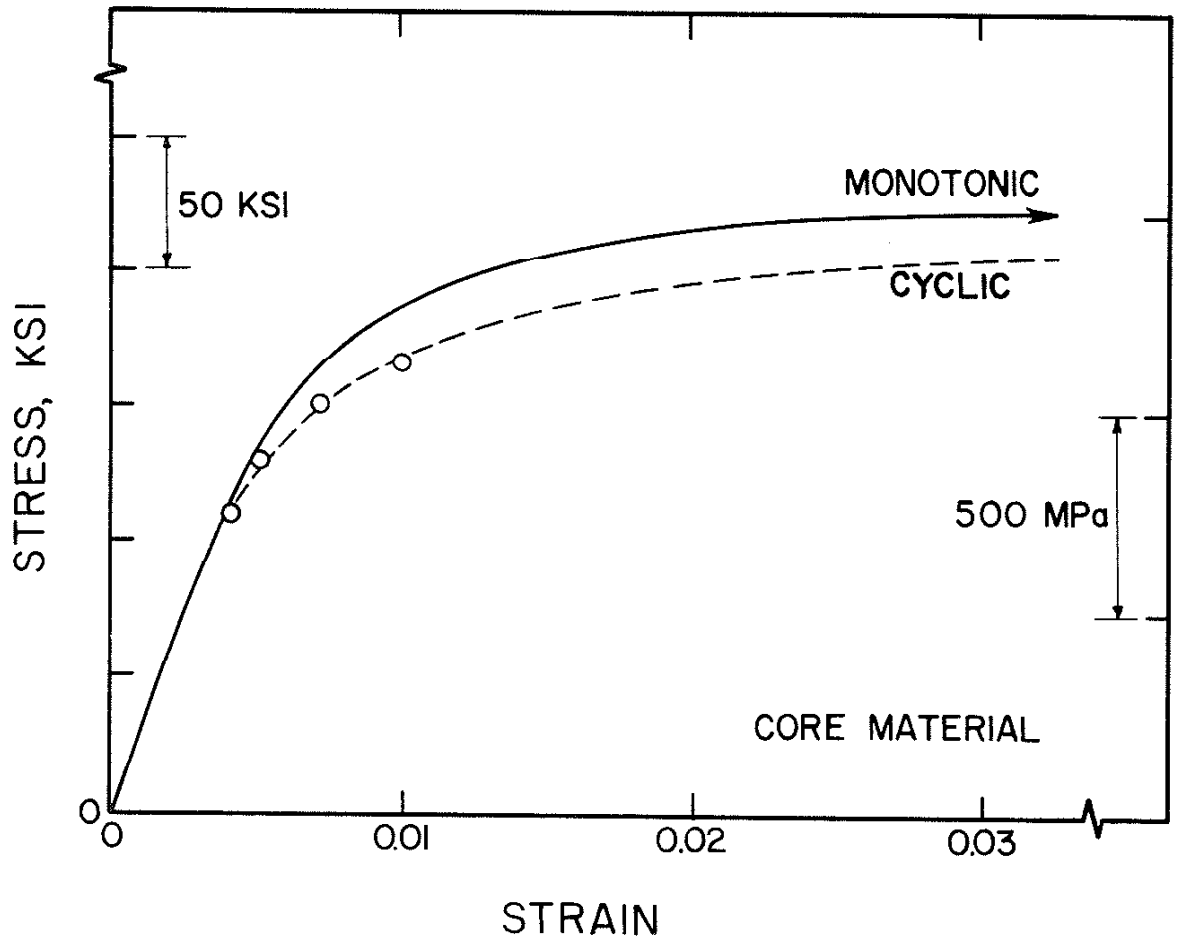


FIG. 10 MONOTONIC AND CYCLIC STRESS-STRAIN CURVES FOR SIMULATED CORE MATERIAL

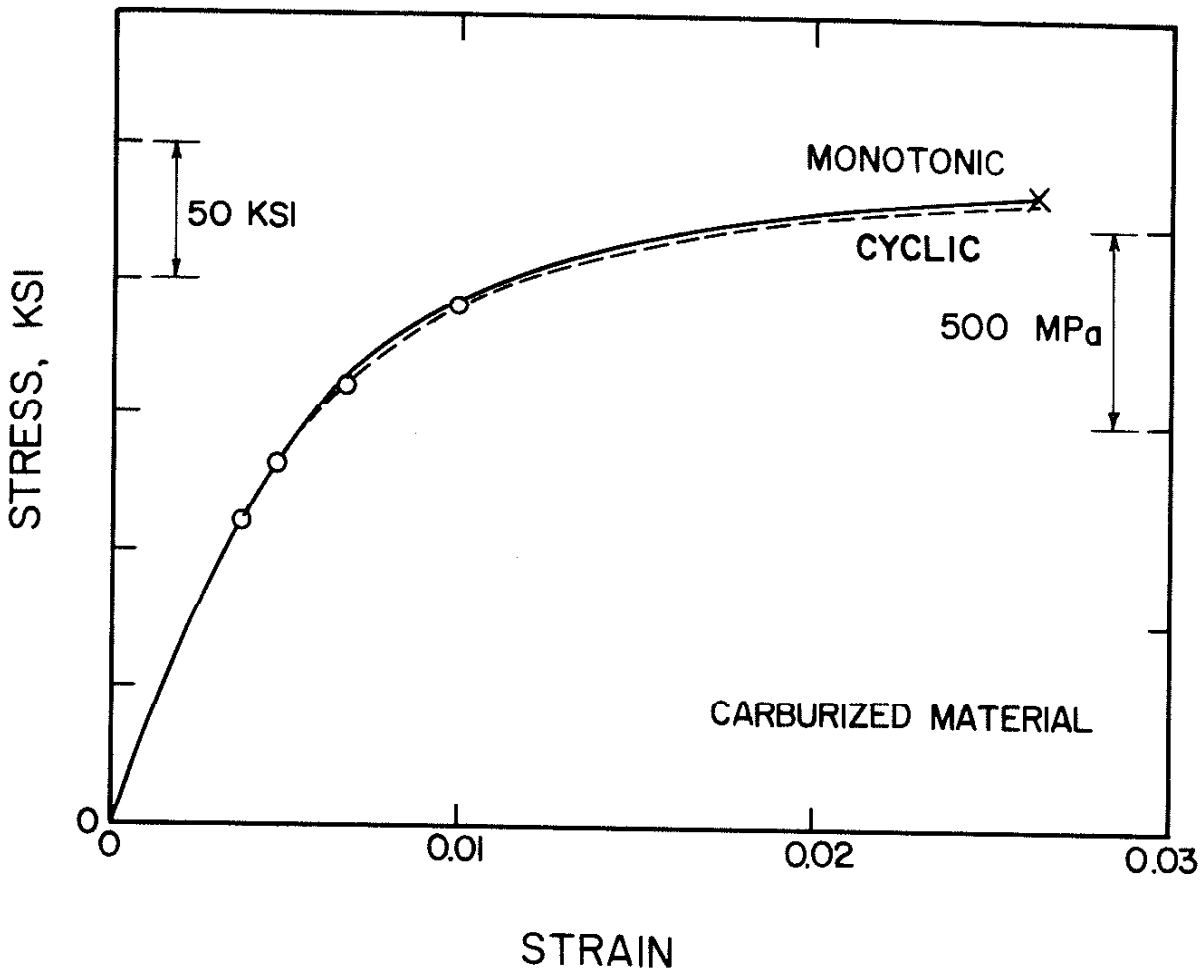


FIG. 11 MONOTONIC AND CYCLIC STRESS-STRAIN CURVES FOR CARBURIZED MATERIAL

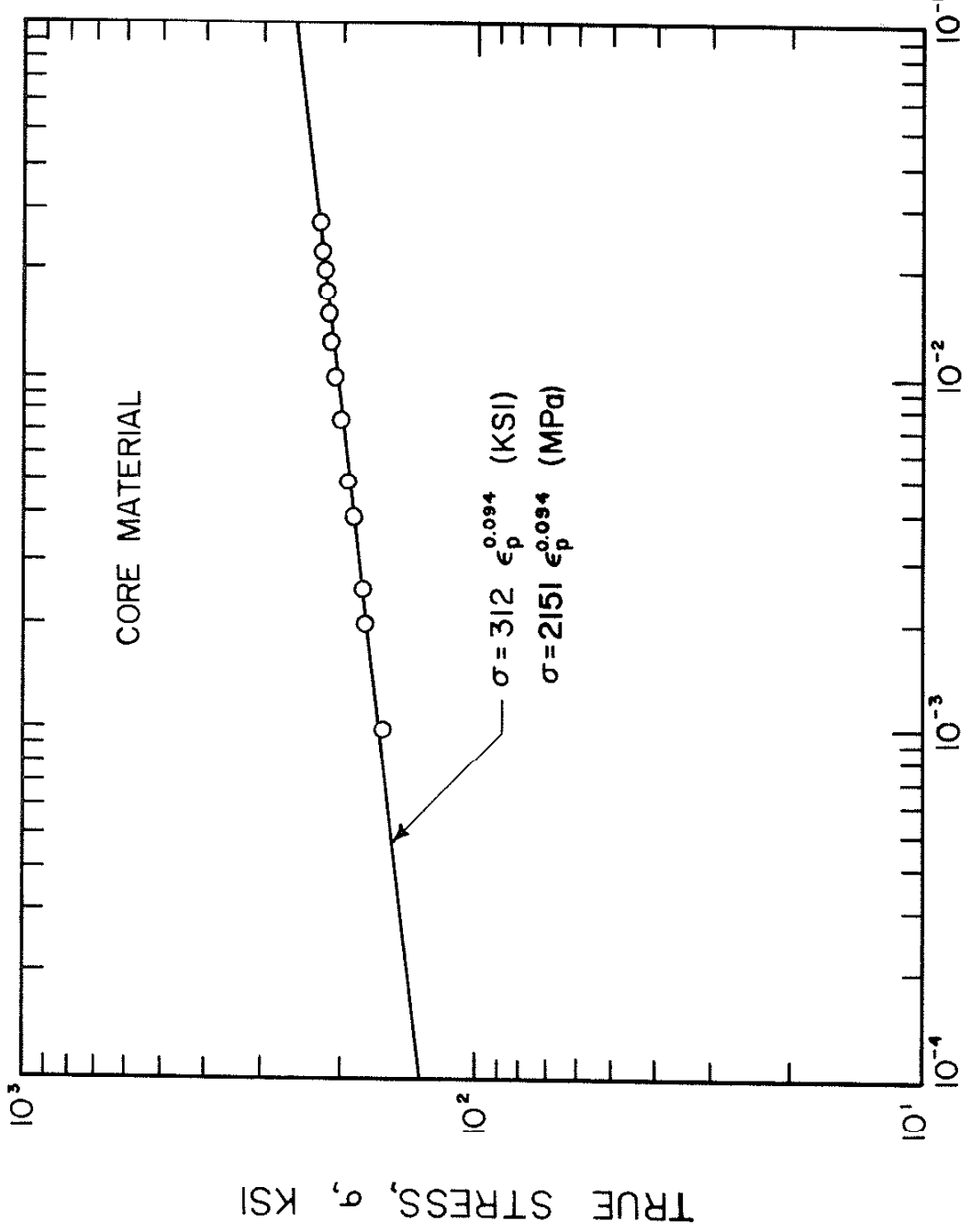


FIG. 12 TRUE STRESS-PLASTIC STRAIN CURVE FOR SIMULATED CORE MATERIAL

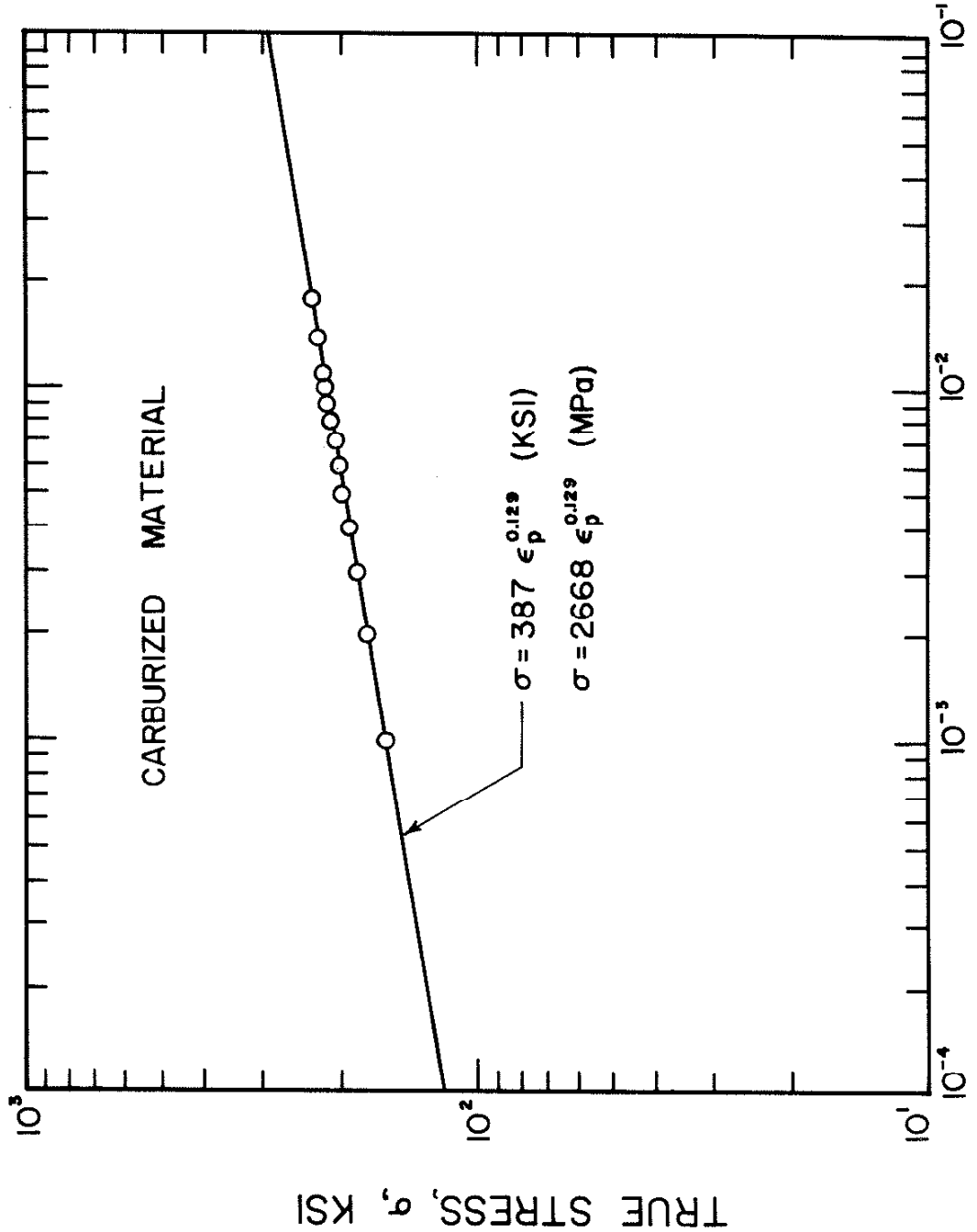


FIG. 13 TRUE STRESS-PLASTIC STRAIN CURVE FOR CARBURIZED MATERIAL

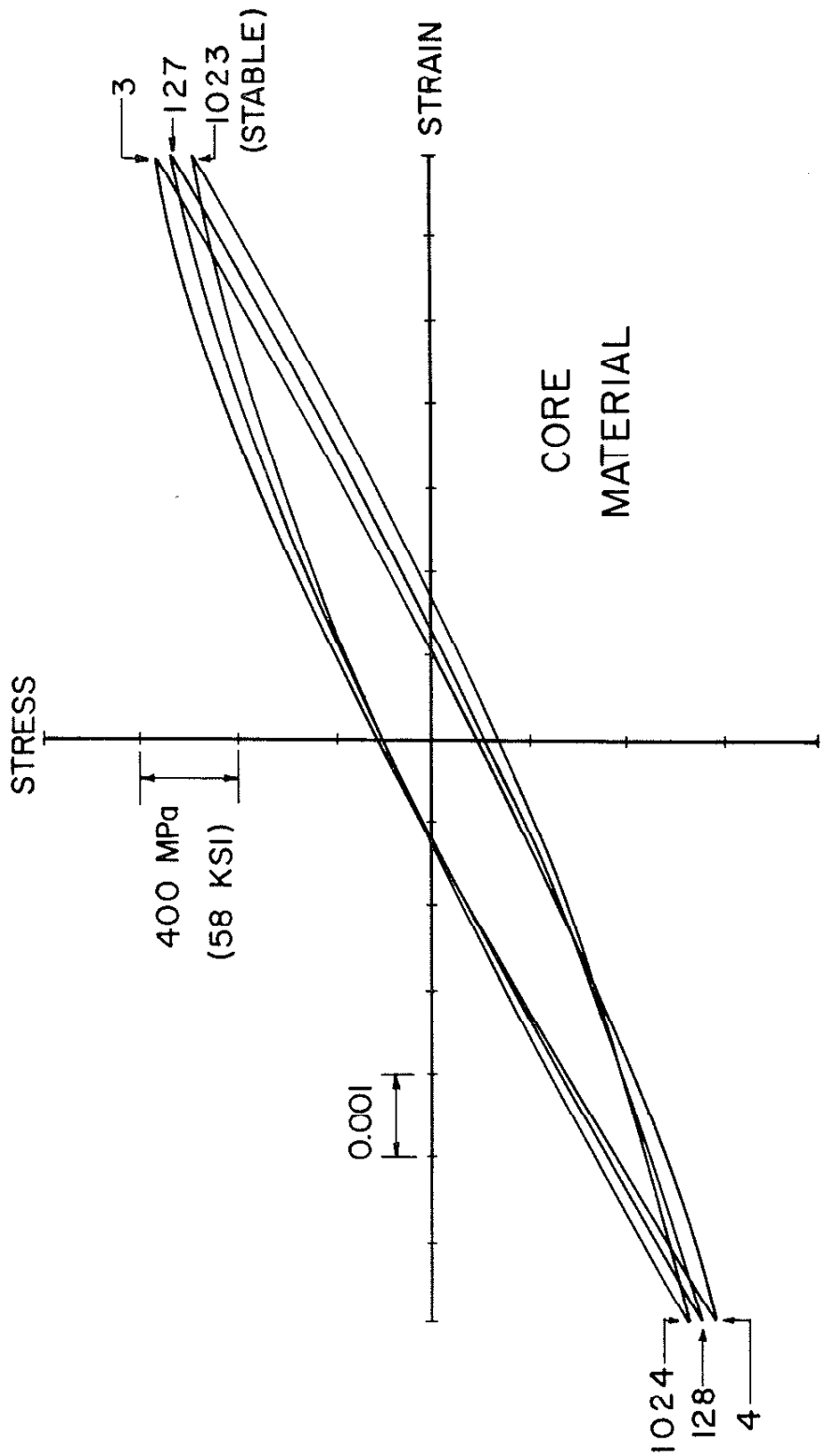


FIG. 14 STRESS-STRAIN RESFONSE OF SIMULATED CORE MATERIAL TO STRAIN CYCLING AT $\Delta\varepsilon/2 = 0.007$. LOOP TIPS ARE LABELLED WITH THE REVERSAL NUMBER.

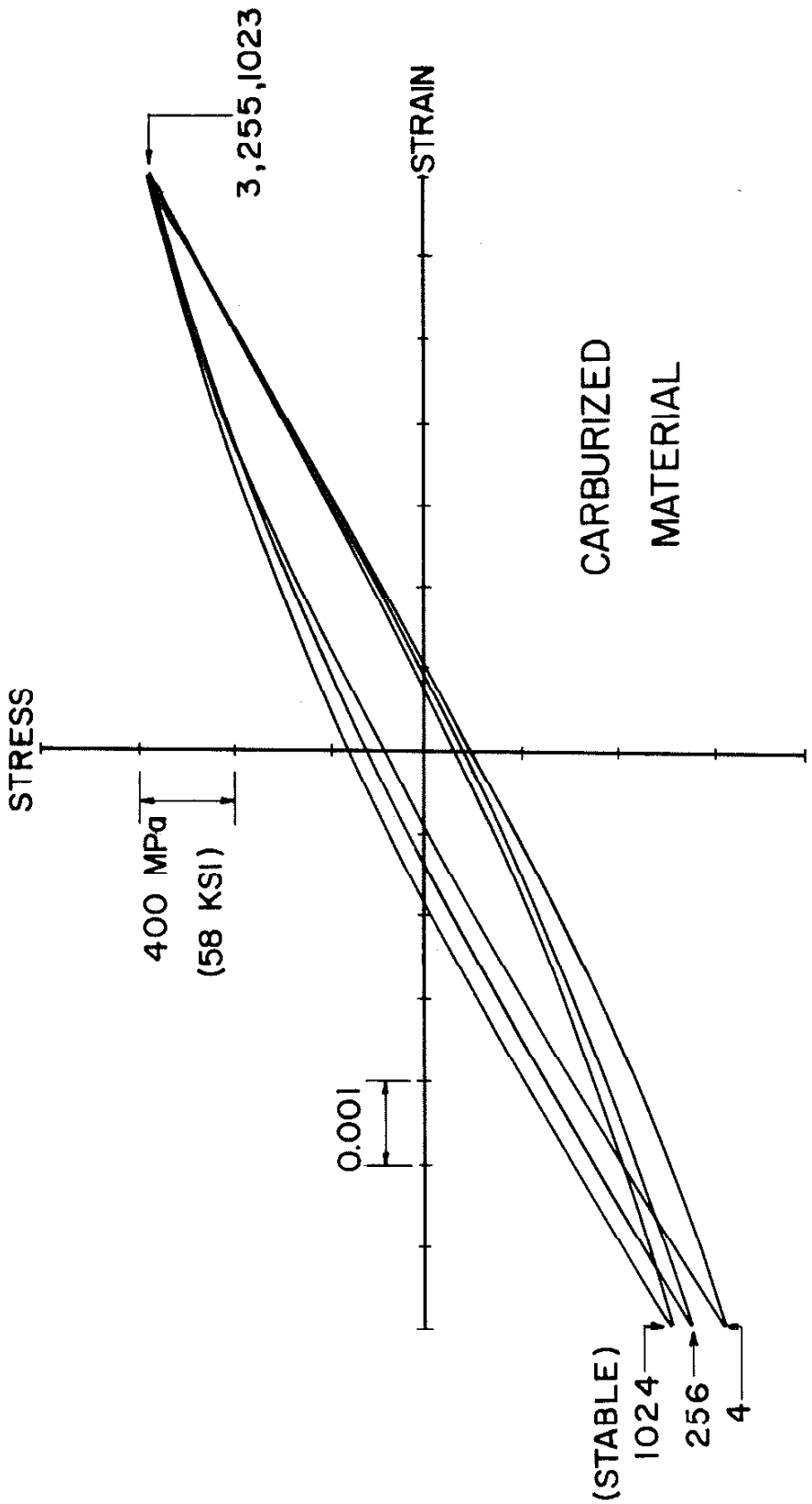


FIG. 15 STRESS-STRAIN RESPONSE OF CARBURIZED MATERIAL TO STRAIN CYCLING AT $\Delta\varepsilon/2 = 0.007$. LOOP TIPS ARE LABELLED WITH THE REVERSAL NUMBER.

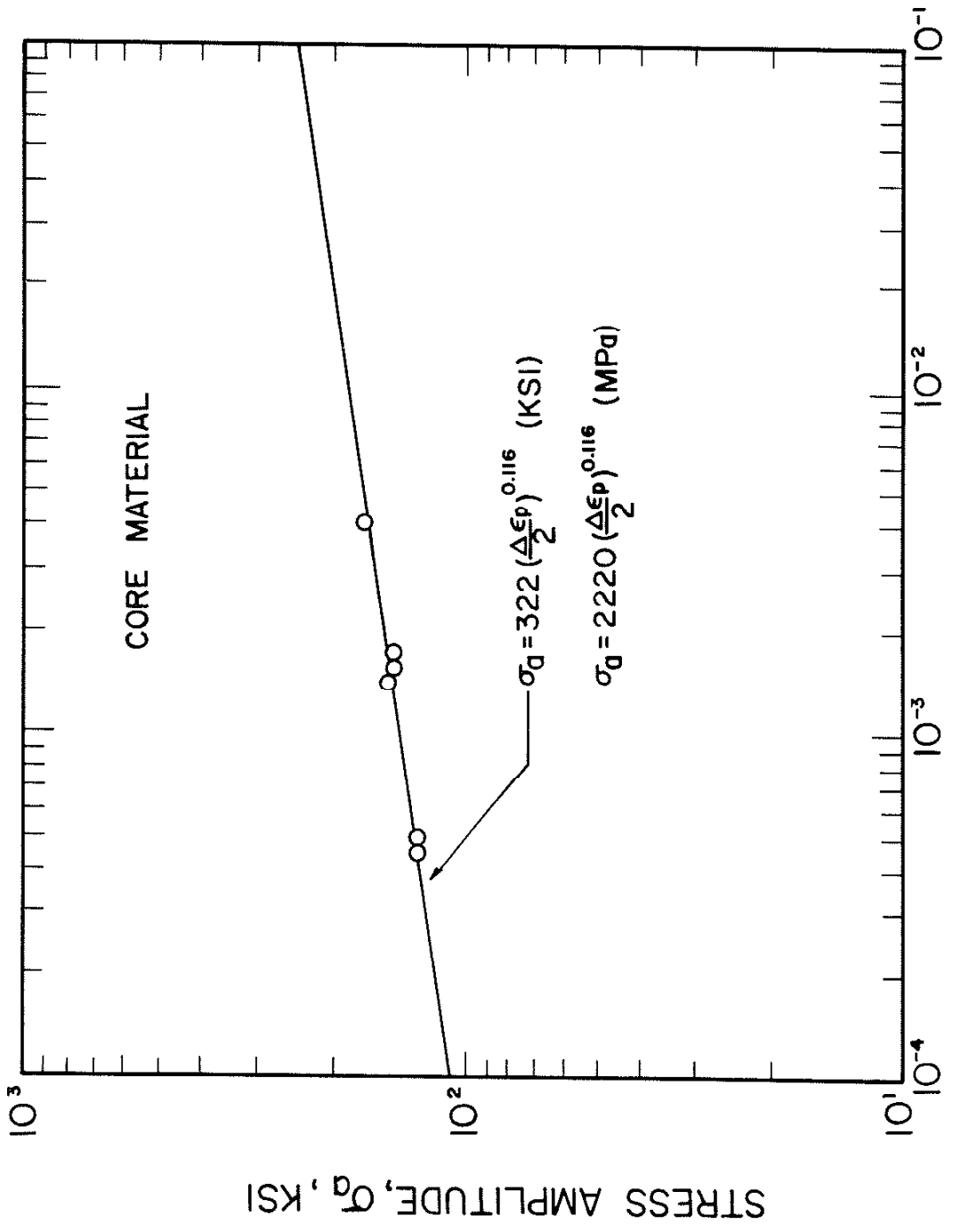


FIG. 16 STRESS AMPLITUDE-PLASTIC STRAIN AMPLITUDE DATA FOR SIMULATED CORE MATERIAL

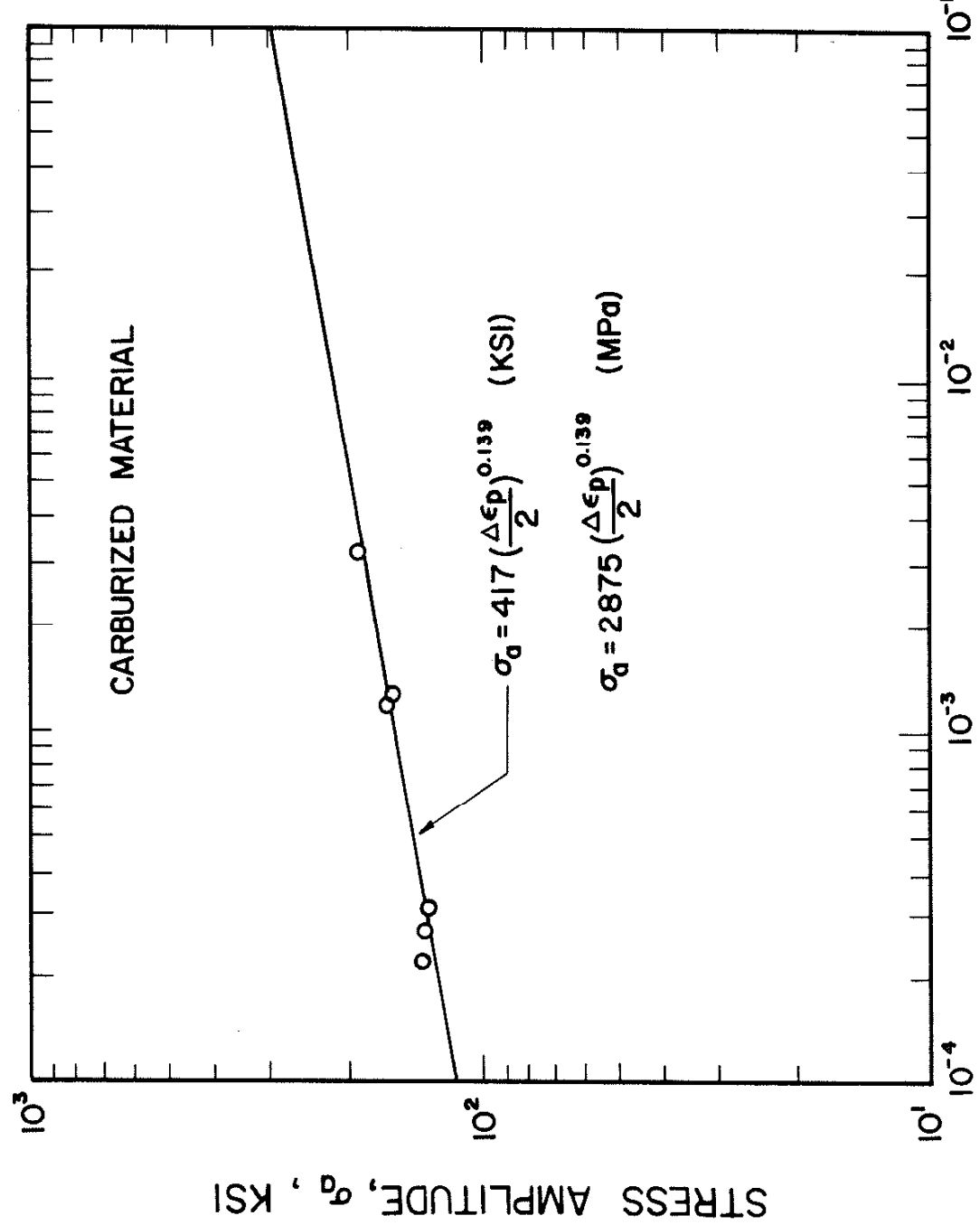


FIG. 17 STRESS AMPLITUDE-PLASTIC STRAIN DATA FOR CARBURIZED MATERIAL

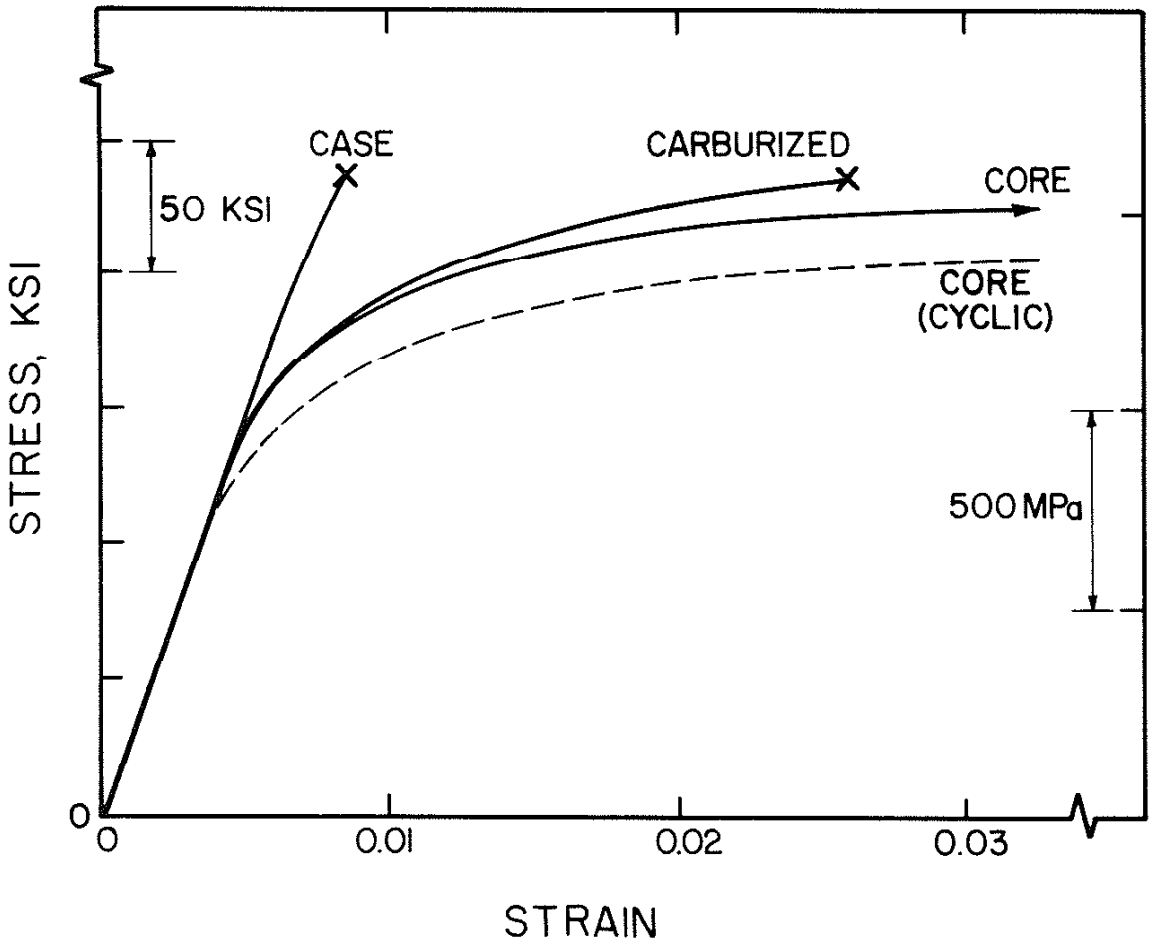


FIG. 18 MONOTONIC AND CYCLIC STRESS-STRAIN CURVES FOR CASE, CORE AND CARBURIZED MATERIALS (NOTE: CARBURIZED MATERIAL IS CYCLICALLY STABLE)

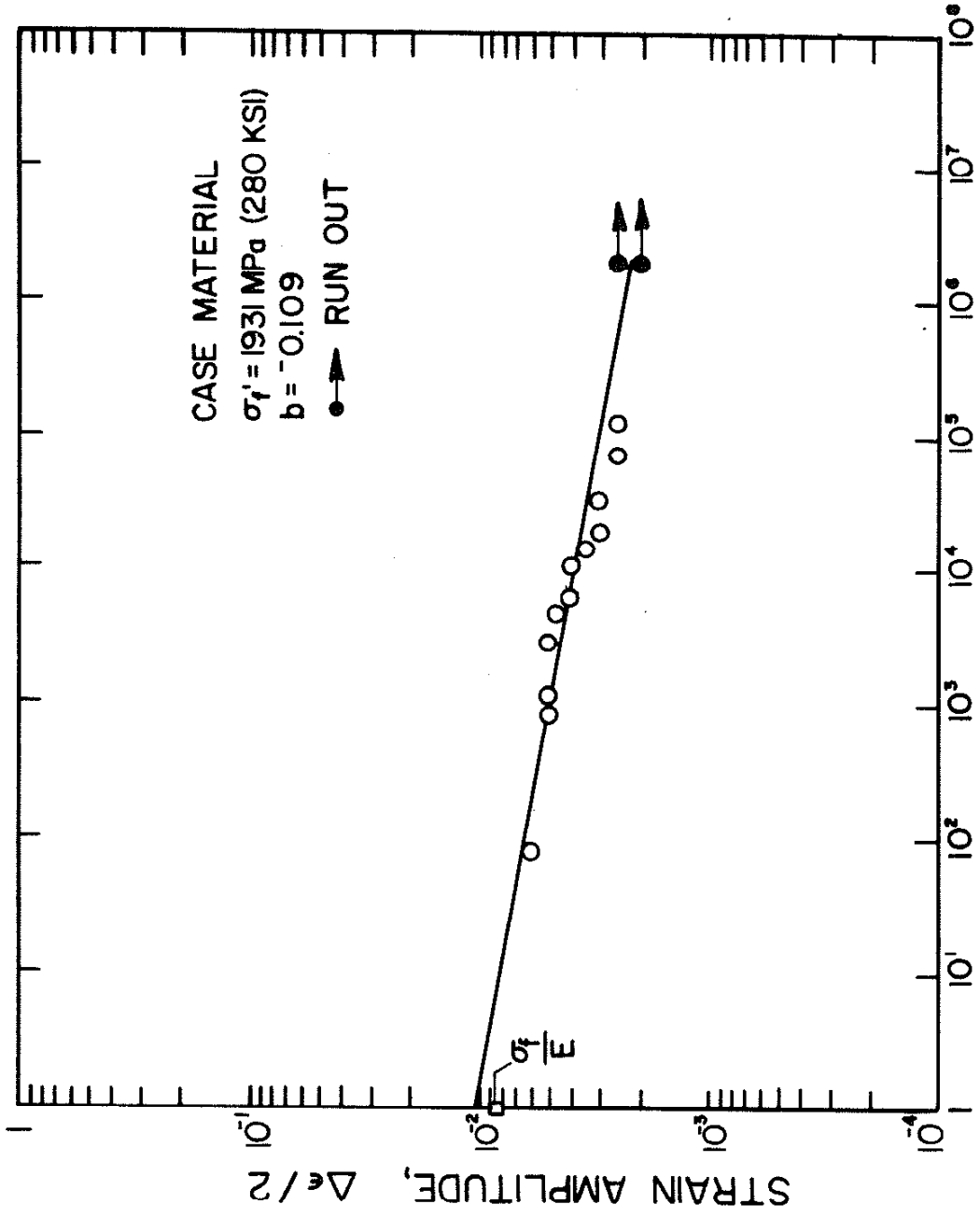


FIG. 19 STRAIN AMPLITUDE-REVERSALS TO FAILURE DATA FOR SIMULATED CASE MATERIAL

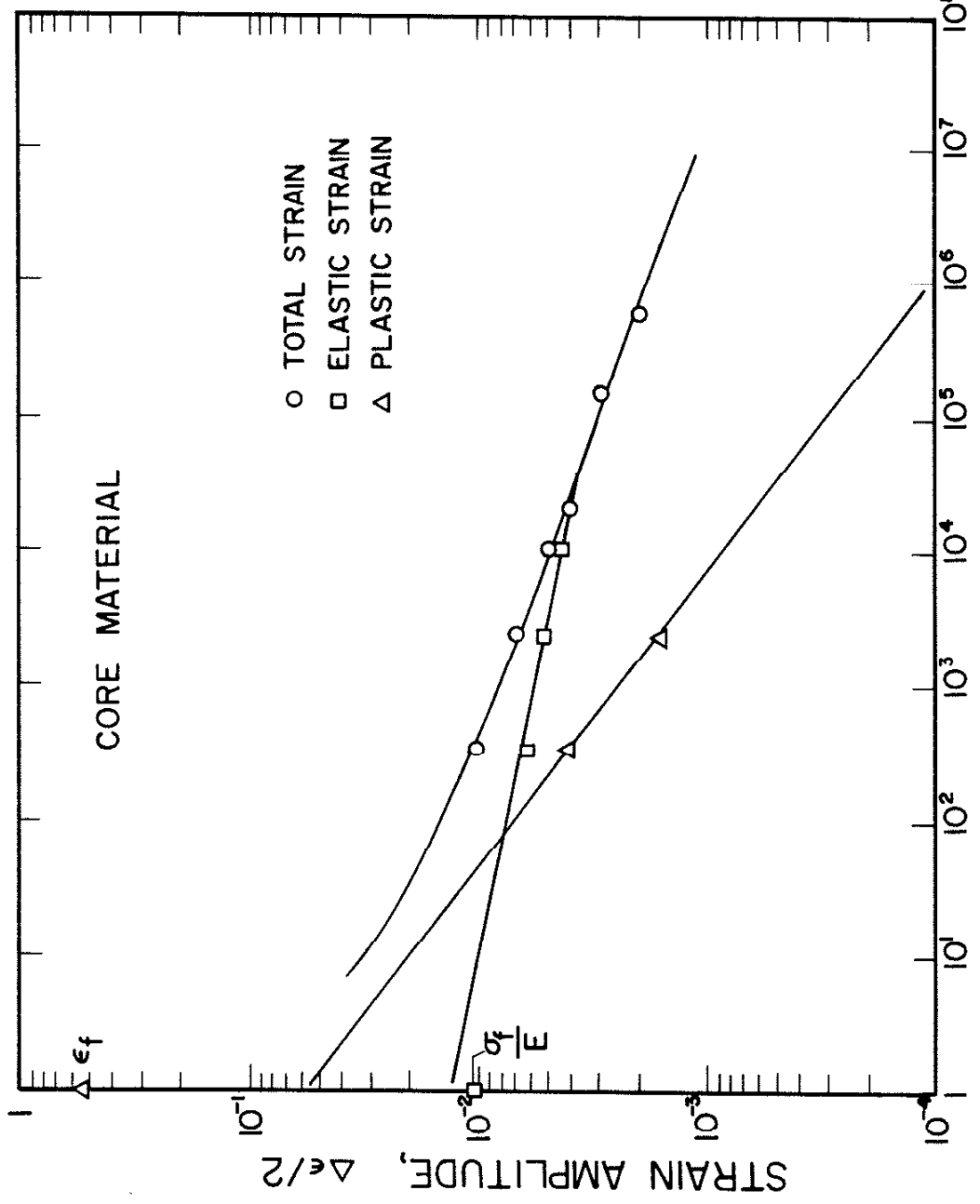


FIG. 20 STRAIN AMPLITUDE-REVERSALS TO FAILURE DATA FOR SIMULATED CORE MATERIAL

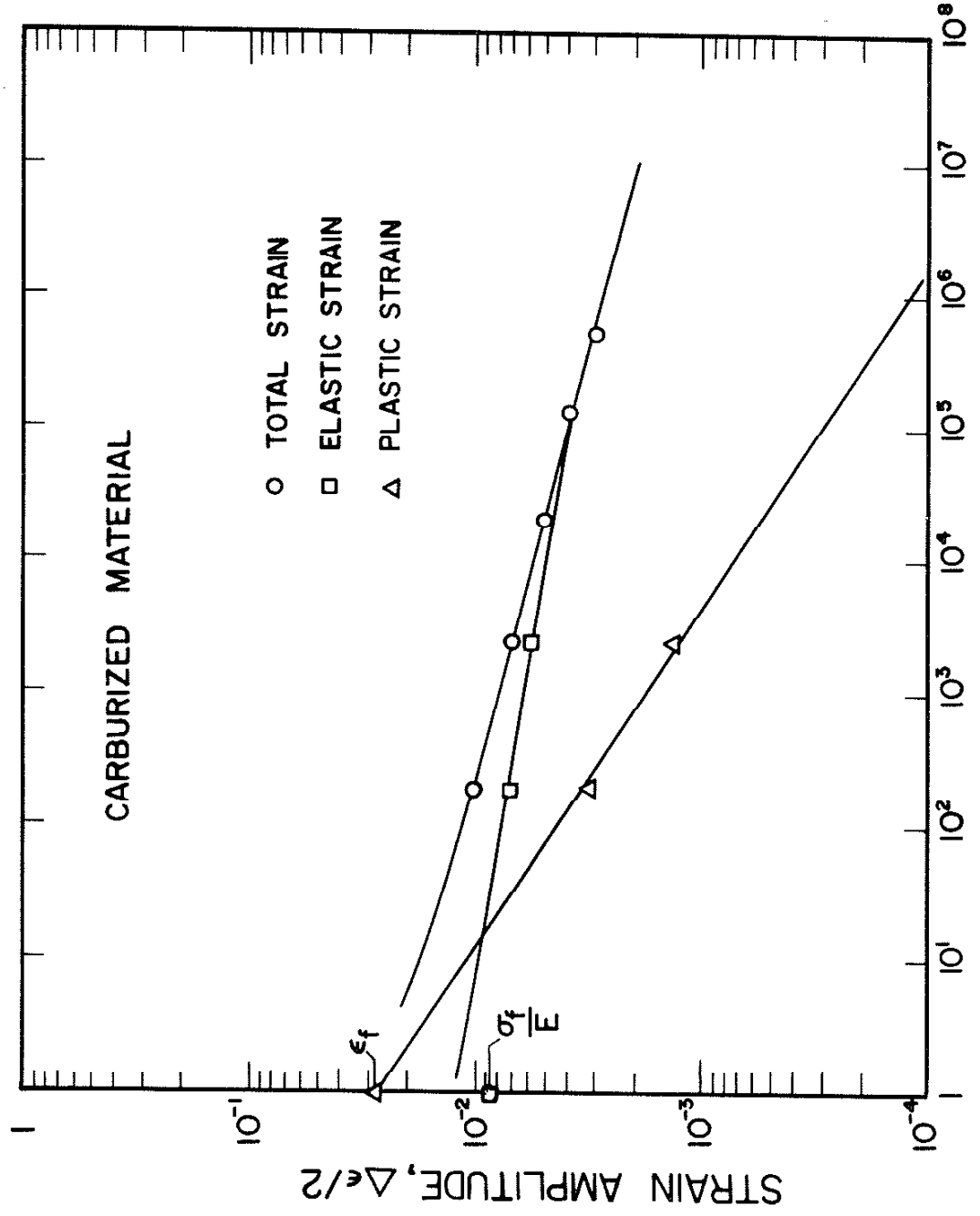


FIG. 21 STRAIN AMPLITUDE-REVERSALS TO FAILURE DATA FOR CARBURIZED MATERIAL

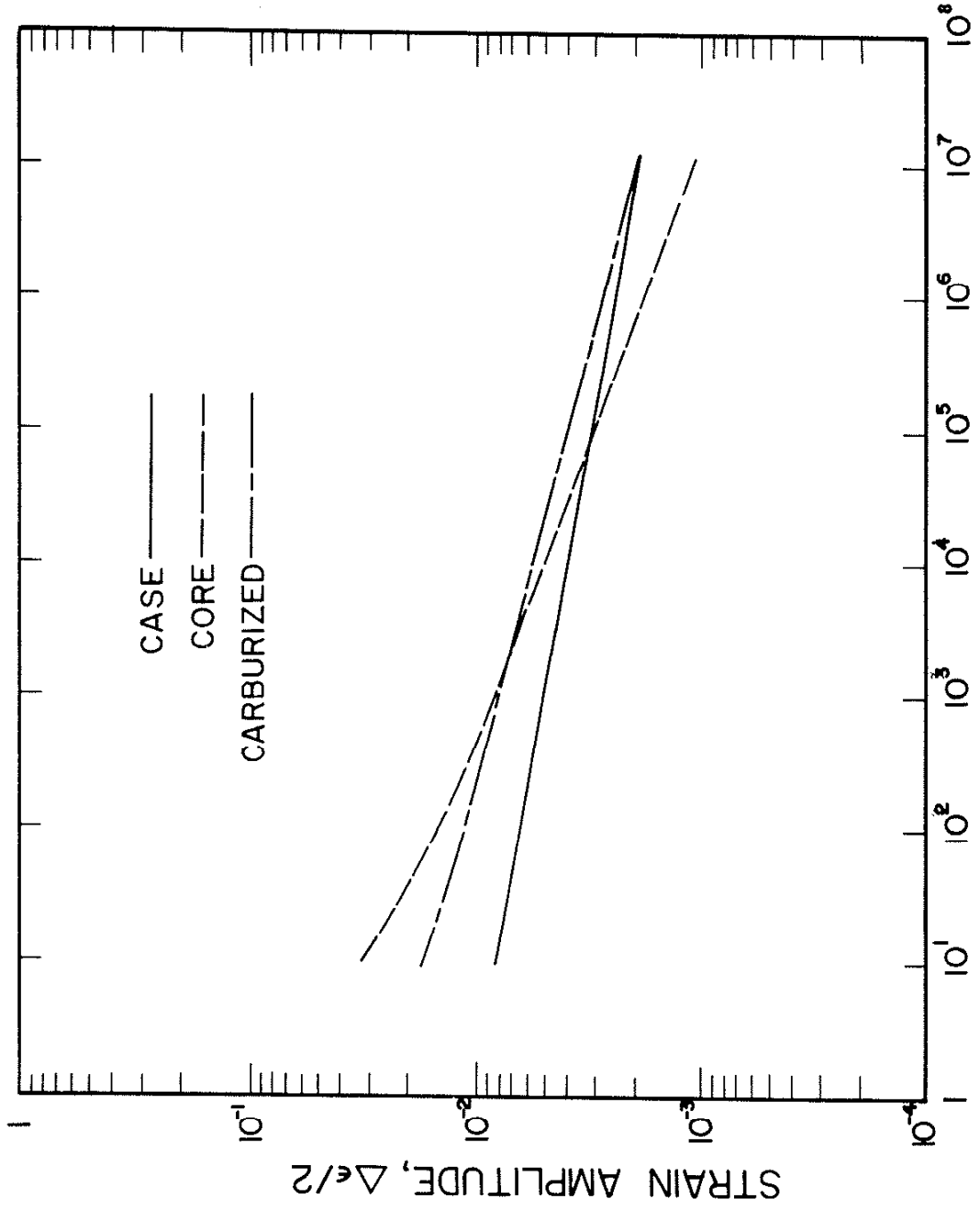


FIG. 22 SUMMARY PLOTS OF TOTAL STRAIN AMPLITUDE-REVERSALS TO FAILURE DATA FOR CASE, CORE AND CARBURIZED MATERIALS

# APPENDIX A

## CRACK GROWTH TEST REPLICATING TECHNIQUE

The procedure for obtaining replicas of a specimen in strain control mode is presented. Photographs of replicas showing the propagation of fatigue cracks during one crack growth test are shown in Fig. A-1. Crack length - reversals data for this same test are shown in Fig. A-2.

1. Test performed in strain control mode
2. Record hysteresis loop
3. Go to zero strain on "down" side of hysteresis loop
4. Record load $P = P^*$ at strain $\varepsilon = 0$
5. In strain control, go to $P = 0$, record $\varepsilon = \varepsilon^*$
6. Hydraulics off
7. Remove extensometer
8. Select load control mode
9. Check set point
10. Hydraulics on
11. Go to replicating load
12. Take replicas
13. Return to $P = 0$
14. Remount extensometer
15. Set offset on extensometer with amplifier zero control to strain reading of $\varepsilon^*$
16. Hydraulics off
17. Select strain control mode
18. Check set point
19. Hydraulics on
20. At $\varepsilon = 0$ check for $P = P^*$
21. Resume test if $P = P^*$

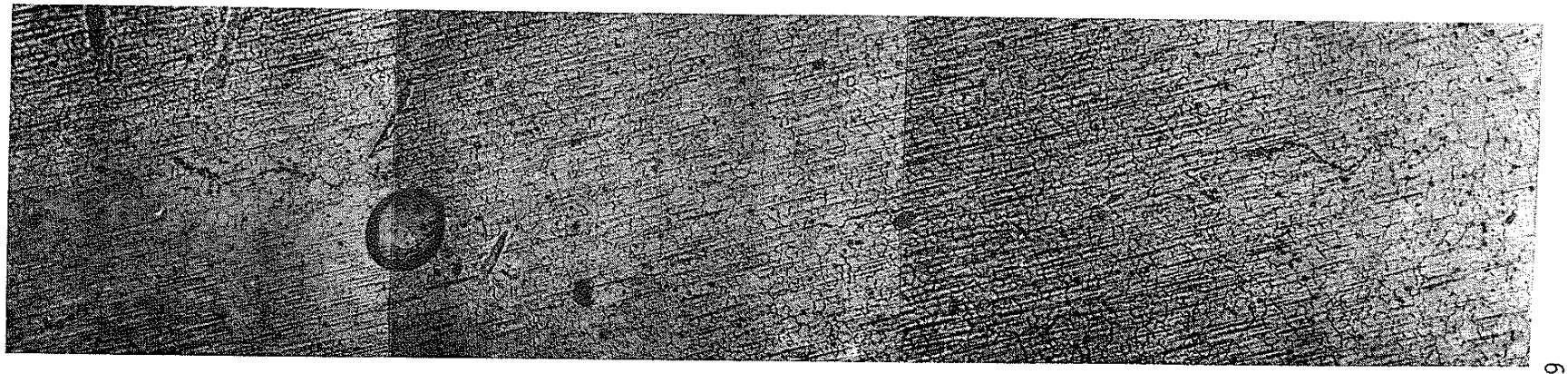

LOADING AXIS

(a) 900 REVERSALS

0.01 in
0.254 mm

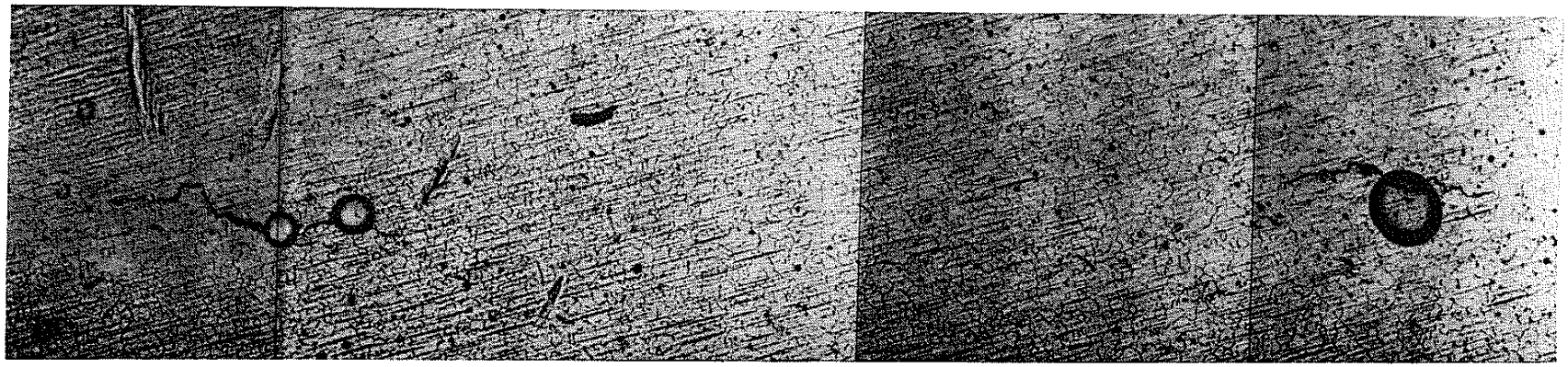

(b) 1200 REVERSALS

FIG. A-1 PHOTOGRAPHS OF REPLICAS SHOWING PROPAGATION OF FATIGUE CRACKS, CRACK NO. 1 IS ON THE LEFT. (SPECIMEN NO. D79-31, $\Delta\epsilon/2$ = 0.007, FAILED AT 1940 REVERSALS)

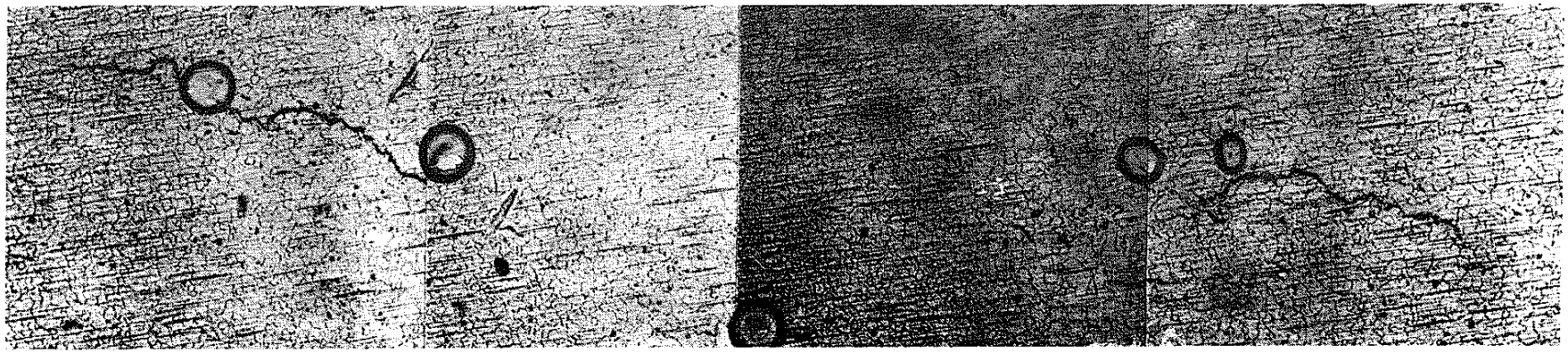

↕ LOADING AXIS

(c) 1500 REVERSALS

0.01 in
0.254 mm

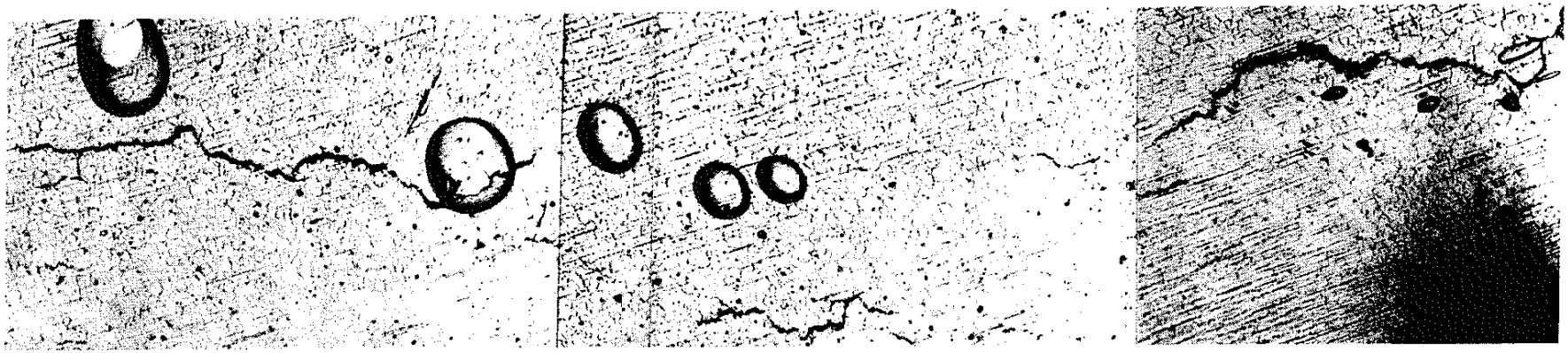

(d) 1800 REVERSALS

FIG. A-1 PHOTOGRAPHS OF REPLICAS SHOWING PROPAGATION OF FATIGUE CRACKS, CRACK NO. 1 IS ON THE LEFT. (SPECIMEN NO. D79-31, $\Delta\varepsilon/2 = 0.007$, FAILED AT 1940 REVERSALS)

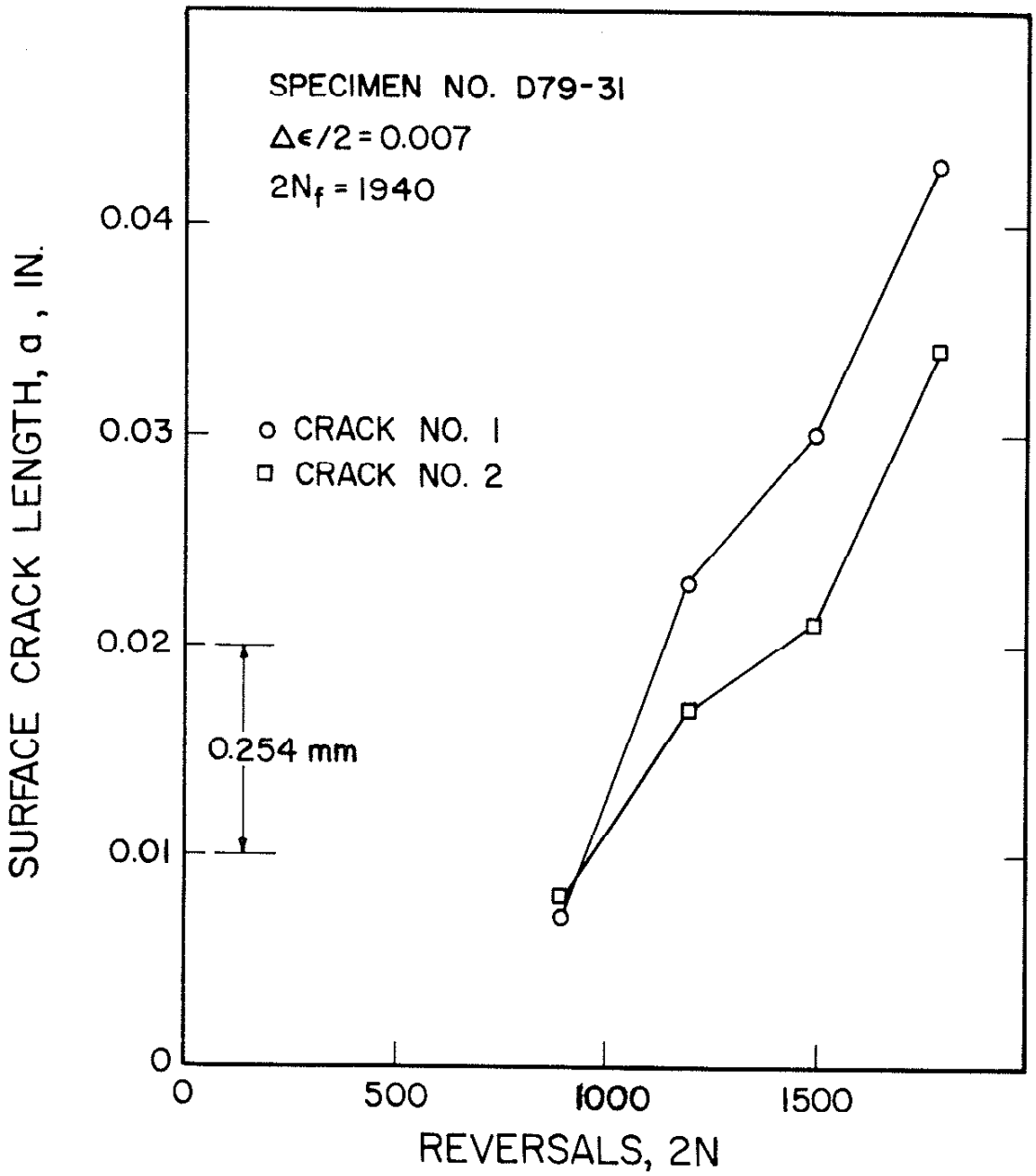


FIG. A-2 CRACK LENGTH-REVERSALS DATA OBTAINED FROM SURFACE REPLICAS

# APPENDIX B

## FRACTURE SURFACE APPEARANCE OF CASE, CORE AND CARBURIZED MATERIALS

Fractographs illustrating general macroscopic surface features are presented for simulated case, simulated core and carburized materials. The effects of hardness and carbon content on fracture appearance can be seen by comparing the fractographs of case and core material. The extent of the shear lip zone is considerably less for case material as would be expected on the basis of decreasing ductility. The macroscopic fracture surface in the case region of carburized material subjected to monotonic tension is quite flat and featureless. Fracture through the core region is dull and fibrous, which is often characterized by ductile microvoid coalescence.

Fractographs representative of case, core and carburized specimens fatigued at a strain amplitude of 0.004 exhibit several interesting features. The case material fracture surface is again relatively flat and featureless, while the core material fracture surface is quite irregular. The fatigue fracture surface of carburized material shows a subsurface failure initiation. Compressive residual stresses in the surface layers of carburized material effectively offset surface weaknesses, so that fatigue cracks are seen to propagate internally. The internal defect responsible for this subsurface failure appears to be either an inclusion or a void.

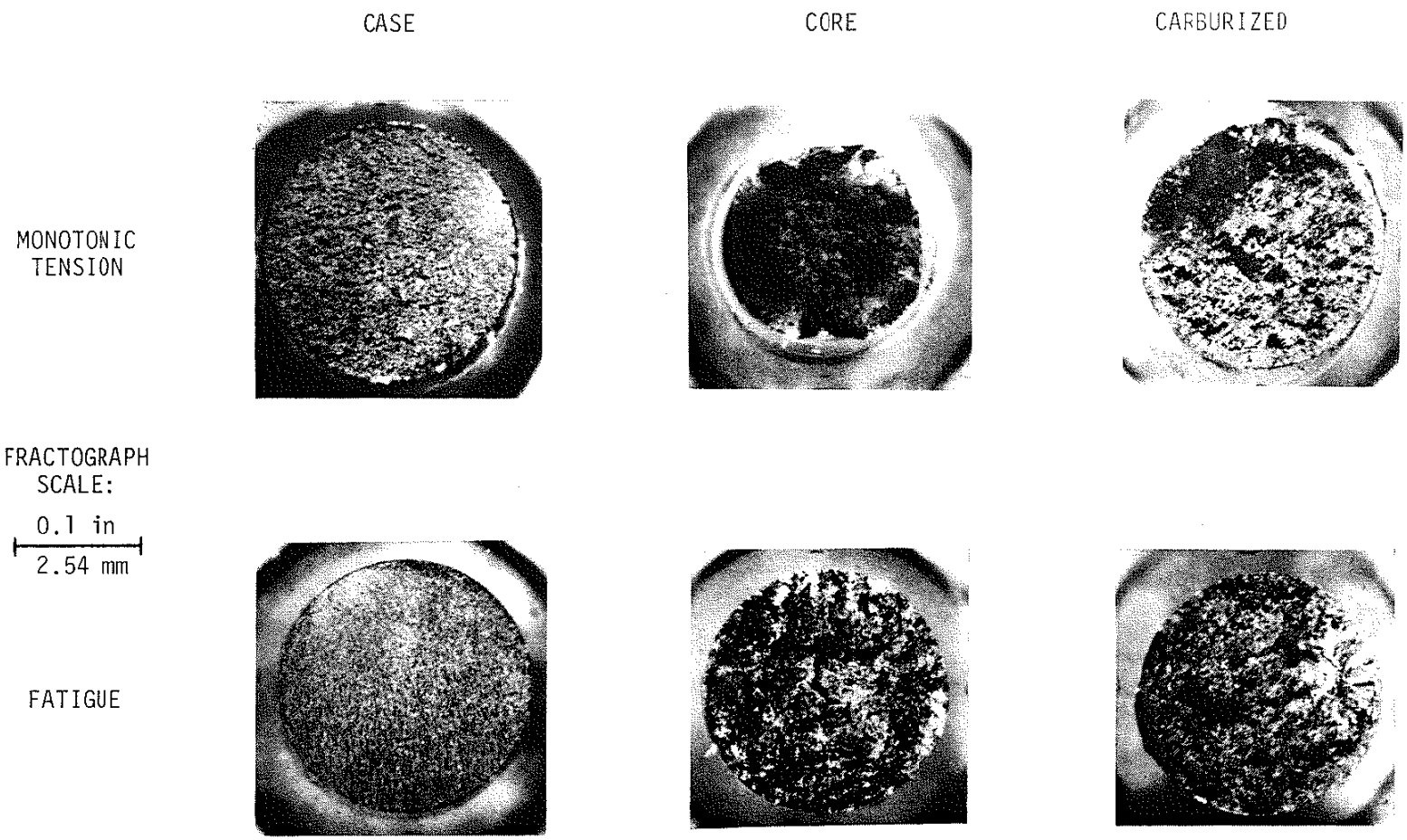


FIG. B-1 FRACTOGRAPHS OF SIMULATED CASE, SIMULATED CORE AND CARBURIZED MATERIALS